Deltares

DWSM-Mud: a sixth-generation 3D model of the Dutch Wadden Sea for hydrodynamics and mud dynamics

2023 release

DWSM-Mud: a sixth-generation 3D model of the Dutch Wadden Sea for hydrodynamics and mud dynamics
2023 release

Auteur(s)
Roy van Weerdenburg

DWSM-Mud: a sixth-generation 3D model of the Dutch Wadden Sea for hydrodynamics and mud dynamics
2023 release

Client	Rijkswaterstaat Water, Verkeer en Leefomgeving
Contact	mevrouw M. Heldring
Reference	
Keywords	D-HYDRO, D-Flow Flexible Mesh, D-Water Quality, Wadden Sea, DWSM, hydrodynamic model, mud dynamics; fine sediment modelling

Document control	
Version	1.0
Date	03-04-2024
Project nr.	11209231-001
Document ID	11209231-001-ZKS-0002
Pages	70
Classification	
Status	definitief

Author(s)		
	Roy van Weerdenburg	

Summary

Upon request of Rijkswaterstaat (RWS), Deltares has developed a sixth-generation three-dimensional hydrodynamic model of the Dutch Wadden Sea, including the Ems-Dollard estuary and a part of the North Sea immediately north and west of the Wadden Sea. The hydrodynamic model is expanded with a set of processes to simulate fine sediment dynamics in the Dutch Wadden Sea.

The development of this model is part of a more comprehensive project in which sixth-generation models have been developed for all waters maintained by RWS. An important difference with the previous fifth-generation models is the use of the D-HYDRO Suite (known internationally as the Delft3D Flexible Mesh Suite), the new software framework for modelling free surface flows, which was first released in 2015 and allows for the use of unstructured grids.

During the initial Dutch Wadden Sea Model (DWSM) model development, preliminary versions of the larger domain Dutch Continental Shelf Models (DCSM-FM 100m and 3D DCSM-FM) were used. An assessment of the impact of recent developments of those large domain models to the results of DWSM made clear that several improvements needed to be included in a new, second version of DWSM.

The new hydrodynamics-only release was developed and validated within KPP Modelschematisaties 2022. The model was updated with respect to the model bathymetry, tidal boundary forcing, meteorological forcing and numerous other adjustments and improvements.

As part of SITO MAD07 Beheer, Onderhoud en Ontwikkeling (BOO) Waterkwaliteitsmodelschematisaties 2023, the DWSM-Mud fine sediment transport model, that was originally developed in 2020, was connected to the updated version of the hydrodynamic model. The set-up and performance of the fine sediment transport model is very similar to what it was in the first release.

The present report deals with the model description of the second release of DWSM-Mud, including the validation results. This report builds upon the description of the hydrodynamic release of DWSM by Zijl et al. (2022).

For external reference purposes, the name *dflowfm3d-waddenzee_200m-j22_6-v1a* is used for the hydrodynamic model. The name *dflowfm3d_dwaq_slib-waddenzee_200m-j22_6-v1a* is used for the combined hydrodynamic and fine sediment transport model.

Contents

1 Introduction

1.1 Background

Upon request of Rijkswaterstaat (RWS), Deltares has developed a sixth-generation three-dimensional hydrodynamic model of the Dutch Wadden Sea, including the Ems-Dollard estuary and a part of the North Sea immediately north and west of the Wadden Sea. The hydrodynamic model is expanded to become applicable to simulate the transport and water-bed exchange of fine sediment in the Dutch Wadden Sea.

The development of this model is part of a more comprehensive project in which sixth-generation models have been developed for all waters maintained by RWS. An important difference with the previous fifth-generation models is the use of the D-HYDRO Suite (known internationally as the Delft3D Flexible Mesh Suite), the new software framework for modelling free surface flows, which was first released in 2015 and allows for the use of unstructured grids.

The development of the first version of this model was initiated in 2019 as a cooperation between three projects (KPP Hydraulica Schematisaties, Waddenfonds Slibmotor Koehoal en KPP Waddenzee Kennisontwikkeling morfologie en baggerhoeveelheden, deelproject KRW-slib) and multiple potential users including hydrodynamicists and fine sediment modellers. The model was initially set up for hydrodynamics only, and later expanded with the inclusion of waves and fine sediment dynamics.

A preliminary version of the hydrodynamic Dutch Wadden Sea model (DWSM) is described by Van Weerdenburg and Zijl (2019). This 3D D-HYDRO Wadden Sea model was built upon schematizations of the Dutch Continental Shelf Model (DCSM-FM) that were available at the time. Later, this model was developed into a combined hydrodynamic and fine sediment transport model through online-coupling with the D-Water Quality process library (Vroom et al., 2020).

1.2 Recent DWSM developments

During the initial DWSM model development, use was made of preliminary versions of DCSM-FM 100m and 3D DCSM-FM. Since these model schematizations were further developed and later officially submitted to Rijkswaterstaat (Zijl et al.; 2020, 2021), it was asked to assess the impact of these further developments, which was reported in Groenenboom (2021). This made clear that several improvements needed to be included in a new, second release of DWSM. The new hydrodynamic release of DWSM was developed and validated within KPP Modelschematisaties 2022 (Zijl et al., 2022). The model was updated with respect to model bathymetry, tidal boundary forcing, meteorological forcing and numerous other adjustments and improvements. For external reference purposes, the name *dflowfm3d-waddenzee_200m-j22_6-v1a* is used for this hydrodynamic model.

The 2022 release of the hydrodynamic model has been developed into a combined hydrodynamic and fine sediment transport model (DWSM-Mud) within SITO MAD07 BOO Waterkwaliteitsmodelschematisaties. For this purpose, much of the 2020 release of the fine sediment transport model (Vroom et al., 2020) has been adopted. The present report deals with the model description and validation for both the hydrodynamics and the sediment transport. For external purposes, the name *dflowfm3d_dwaq_slib-waddenzee_200m-j22_6-v1a* is used for the combined hydrodynamic and fine sediment transport model.

1.3 Guide to this report

This report builds upon the report of the hydrodynamic DWSM model by Zijl et al. (2022). Large parts of the description of the model set-up in Chapter 2 are copied from Zijl et al. (2022), but supplemented by a description of the model setup for wave stirring and fine sediment transport. The description of the hydrodynamic validation in Chapter 3 is a duplicate of Chapter 3 in Zijl et al. (2022). The validation of the fine sediment transport model is discussed in Chapter 4. The report ends with conclusions and recommendations in Chapter 5.

2 Model setup

2.1 Introduction

Originally, the idea was to base DWSM on two other model schematizations:

- The two-dimensional DCSM-FM 100m model. From this model a cut-out of the horizontal schematization is taken by prescribing the area ('enclosure') outside of which the DCSM-FM 100m schematization is ignored.
- The three-dimensional 3D DCSM-FM model. From this model, with a ~900 m resolution in the southern North Sea, the lateral boundary conditions, meteorological surface forcing as well as 3D numerical and physical settings are obtained.

Since the resulting model turned out to be too computationally heavy for subsequent fine sediment simulations, two adjustments were made to this approach. Firstly, the horizontal network was coarsened by omitting the last refinement step of the DCSM-FM 100m network, resulting in a resolution of ~200m in the Wadden Sea. Secondly, the vertical resolution was decreased from 20 to 10 sigma layers.

The DWSM hydrodynamic model in D-Flow FM is expanded to a combined hydrodynamic and fine sediment transport model by adding wave stirring and the computation of mud dynamics via a coupling with the D-Water Quality process library.

2.2 Network

2.2.1 Network coverage, horizontal extent

The model domain of DWSM includes the Dutch Wadden Sea, the Ems-Dollard estuary and the adjacent part of the southern North Sea. The western, northern, eastern and southern offshore boundaries are located at 4° E, 53.975° N, 7.3875° E and 52.55° N, respectively (see Figure 2.1). The southern boundary is located just north of the port of IJmuiden. The network is specified in geographical coordinates (WGS84).

2.2.2 Horizontal grid size

The computational grid is a cut-out of the DCSM-FM 100m grid, without the final refinement to ~100m cell size. The network resolution is 0.5 nautical mile (nm) x 0.5 nm in the coarsest area, which is located in the north-western corner of the domain and increases in two steps to a resolution of 1/8 nm (~200 m) along all Dutch coastlines and inside the Wadden Sea and Ems-Dollard estuary (Figure 2.1; left). At transitions in resolution triangular grid cells are applied. This is illustrated in Figure 2.1 (right) for part of the Texel Inlet. At least a few rectangular grid cells are located between two transitions to a different resolution. The network has almost 200,000 cells. Roughly 70% of these cells have the highest resolution of ~200 m. The area with the highest resolution is less than half of the model domain, which shows that coarsening towards deeper areas is important to limit the total number of cells in the network.

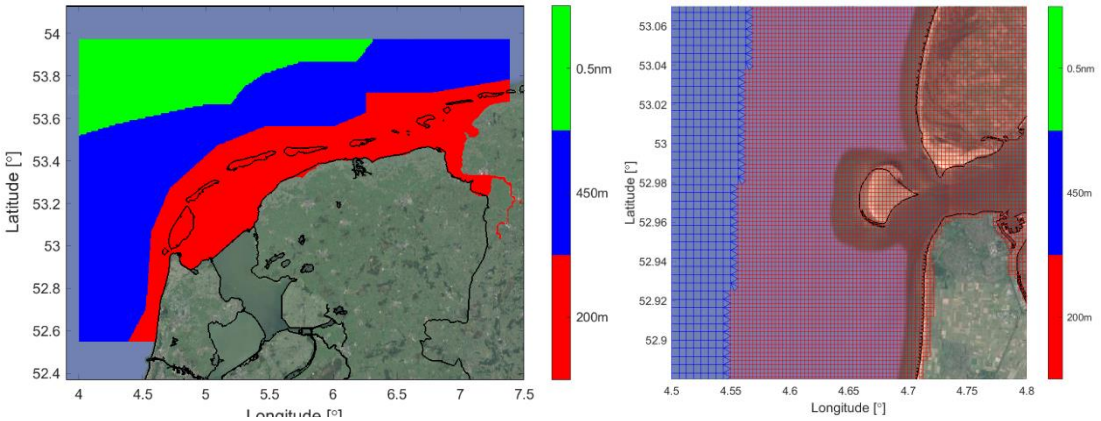

Figure 2.1 Overview (left) and detail (right) of the DWSM model network with the colours indicating the grid size (green: ~0.5 nm; blue: ~0.25 nm; red: ~0.125nm).

2.2.3 Vertical schematization

A sigma-layer approach is used for the vertical schematization of the model. This implies that a fixed number of layers, with a thickness dependent on local water depth, is present. This results in a high vertical resolution in shallow areas. A total of 10 layers with a uniform thickness of 10% of the water column is applied.

2.3 Model bathymetry and geographical features

The model bathymetry and geographical features such as fixed weirs, thin dams and dry points are generated using the Baseline-NL software, an ArcGIS database used for hydrodynamic model development at Rijkswaterstaat. The used (merged) datasets are *baseline-nl_land-j22_6-w1* and *baseline-nl_zee-j22_6-v1*. The bathymetric data in this version is a combination of the gridded bathymetric dataset (December 2020 version) from the European Marine Observation and Data (EMODnet), and Dutch bathymetric data within the Rijkswaterstaat management area. The most recent data from the latter dates from 2021. The model bathymetry is generated from Baseline data by means of grid-cell averaging and is prescribed on the net nodes. A more detailed description of this procedure can be found in Zijl et al. (2022). Figure 2.2 and Figure 2.3 show the model bathymetry for the entire model domain and for the western part of the Wadden Sea, respectively.

Bathymetric data in the Baseline dataset for the shoals in the Eierlandse Zeegat, Vliestroom and Amelander Zeegat has not been updated with the most recent measurements. To use the most accurate data available, in these areas the bed levels are overwritten based on a simple average of a set of LiDAR measurements from 2016 and 2017. The effect of this inclusion of the additional bathymetric data is visualized as the change of the bed level in Figure 2.4. For most shallow areas this results in minor changes of tenths of meters. At the edges of the morphologically more active channels the effect is a bit larger.

Figure 2.5 illustrates the resulting composite of bathymetric survey data that is used to generate the model bathymetry for the Dutch Wadden Sea and the North Sea coast of the Wadden islands. The Baseline data was collected in the period 2019-2021. As mentioned before, LiDAR measurements from 2016 and 2017 (i.e., part of Vaklodingen) are used at the shoals in the Eierlandse Zeegat, Vliestroom and Amelander Zeegat. In deeper parts of the North Sea and in the German Wadden Sea, the EMODNET 2020 data and the Digitale Geländemodelle of Bundesamt für Kartographie und Geodäsie (BKG) are used as input.

Remaining geographical features (fixed weirs, thin dams, dry points and the model enclosure) are identical to those used in this area in the DCSM-FM 100m. However, due to the different resolution of the model grid, the final snapped result differs. Figure 2.6 shows the result at Delfzijl. The Pollendam near Harlingen has been included with floodable fixed weirs.

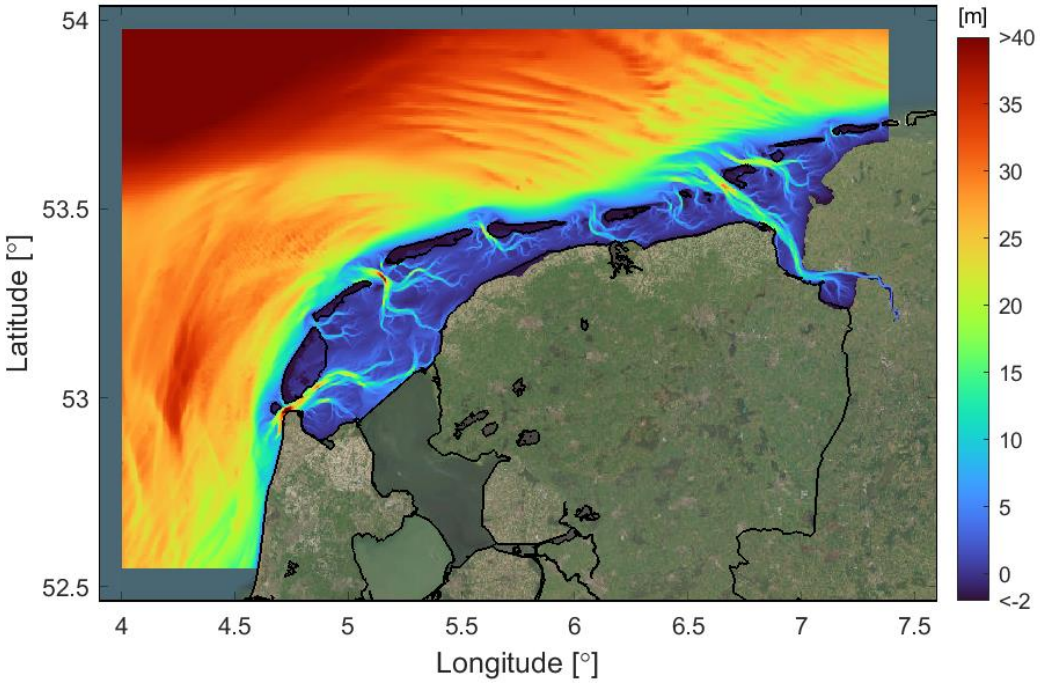

Figure 2.2 Overview of the DWSM model bathymetry (entire model domain).

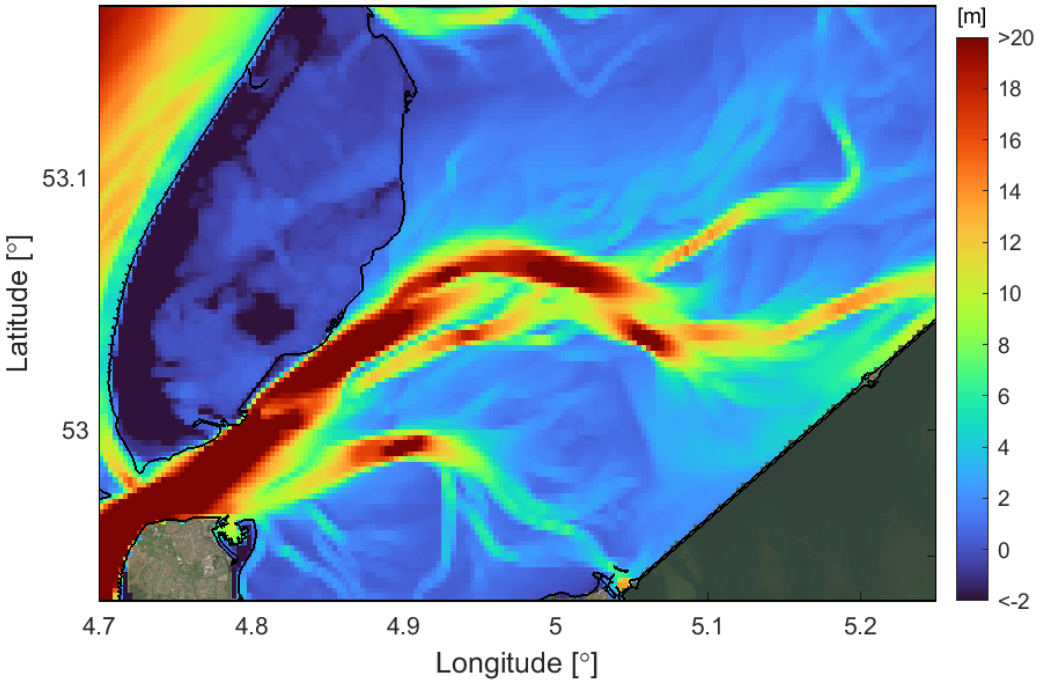

Figure 2.3 DWSM model bathymetry in the western Wadden Sea.

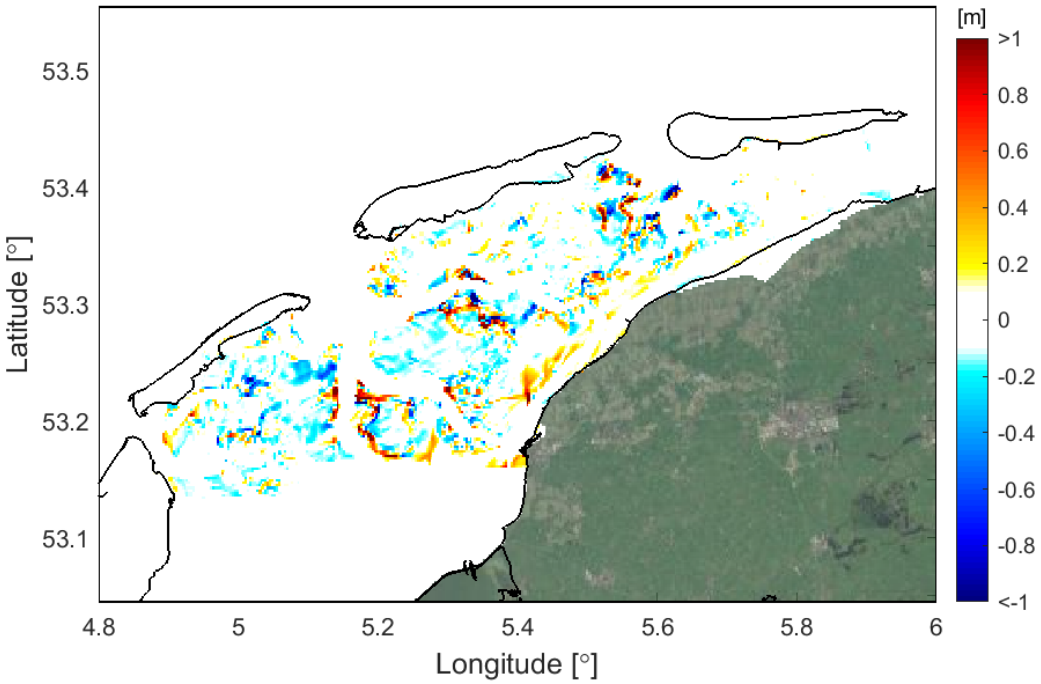

Figure 2.4 Changes in the model bathymetry due to added bathymetric information.

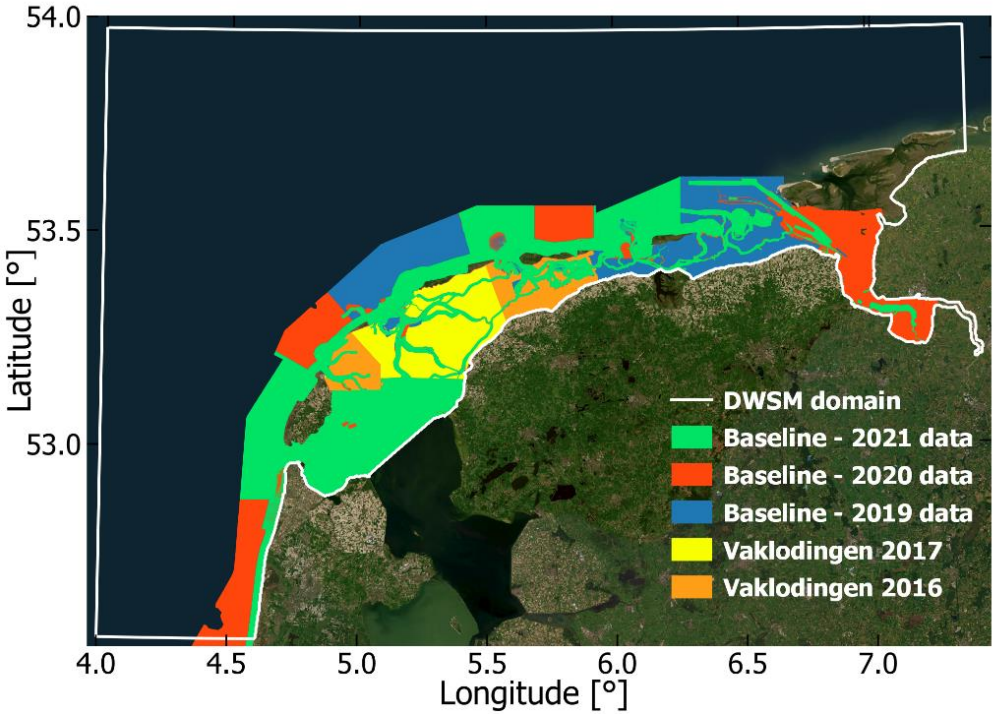

Figure 2.5 Origin of bathymetric data in the Dutch Wadden Sea and along the North Sea coast of the Wadden islands. The Baseline data consists of a combination of 20 m x 20 m and 5 m x 5 m raster data. The Vaklodingen data has a 20 m x 20 m resolution.

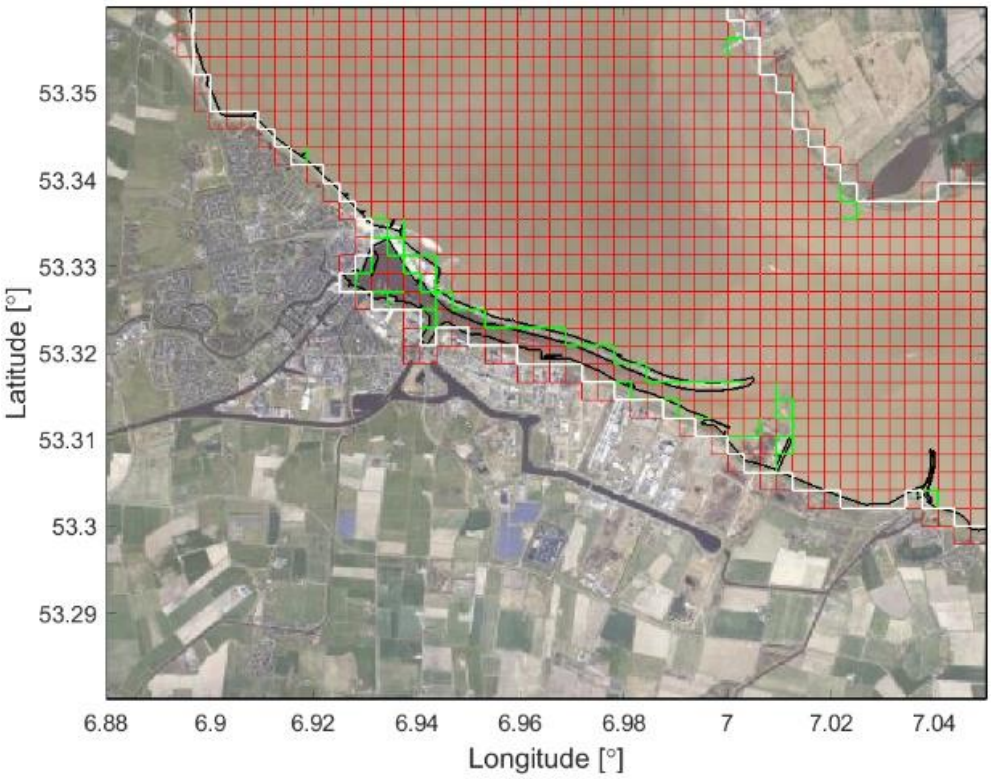

Figure 2.6 Fixed weirs (green) and enclosure (white) on the model grid (red) near Delfzijl after snapping by D-HYDRO.

2.4 Bottom roughness

To account for the effect of bottom friction, a space-varying Manning roughness coefficient is specified. The roughness field used is taken from the 2022 release of DCSM-FM 100m (Zijl et al., 2022a). The values were adjusted to obtain optimal water level representation in the latter model, using the open source data assimilation toolbox OpenDA (Zijl et al., 2022). The roughness fields are not optimized further for the application in the 3D DWSM model and is shown in Figure 2.7.

During the use of an earlier version of this model in fine sediment applications, problems occurred at transitions in roughness value, due to the steepness in roughness gradient in some transition zones and the crossing of important tidal channels. To prevent these issues, the transition zones between roughness areas in the Dutch Wadden Sea were widened and relocated to tidal divides where possible in the 2022 release of DCSM-FM (the model from which the DWSM roughness is taken). For similar reasons, the Wadden Sea roughness areas were expanded to include a larger part of the North Sea coast of the Wadden islands, with the transition to the roughness areas in the North Sea starting from at least the 15 m isobath.

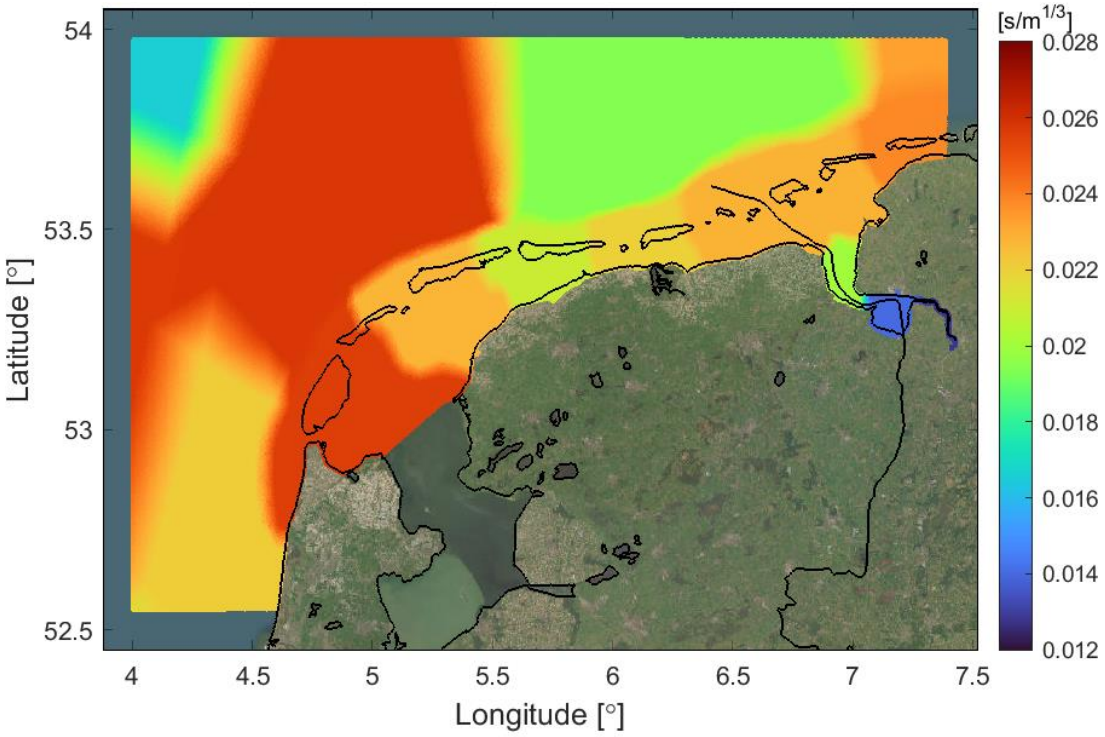

Figure 2.7 Overview of the space-varying Manning bottom roughness field used in DWSM (taken from DCSM-FM 100m).

2.5 Wave stirring

A fetch limited wave model is used to include effects of wave stirring in the mud transport model. The fetch limited wave model that is used is based on the formulations by Hurdle & Stive (1989; *Wavemodelnr = 1*). The implementation of this wave model in Delft3D-FM is discussed in detail by Van Weerdenburg & Hanssen (2023): the wave parameters (i.e., wave height, wave period and wave length) are determined based on the wind conditions (see Section 2.8) and the fetch length and fetch depth. The fetch length and fetch depth are computed every hour, such that the parameters are updated with (tidal) water level variations. This is important in the Wadden Sea, because flooding and drying of intertidal areas may largely affect the fetch length and fetch depth.

The wave model is briefly validated against field measurements of the wave height and wave period at wave buoys. Result of this validation are included in Appendix B.

The computed wave parameters are used in the D-Water Quality process library to determine the total bed shear stress by currents and waves that is used for the entrainment of mud. This total bed shear stress (τ_{total}) is computed as a linear addition of the bed shear stresses by currents and waves:

$$\tau_{total} = \tau_{flow} + \tau_{waves}$$

Non-linear interactions between currents and waves are not taken into account in this (simplified) method.

The bed shear stress by currents equals the friction that is experienced by the flow, following:

$$\tau_{flow} = \frac{1}{2}\rho_w c_f U_b^2$$

in which

U_b the flow velocity near the bed;
c_f a friction coefficient based on the bed roughness (see Section 2.4);
ρ_w the density of the water.

The bed shear stress by waves is computed as:

$$\tau_{waves} = \frac{1}{2}\rho_w f_w U_{orb}^2$$

in which

U_{orb} the orbital velocity near the bed, based on the root-mean square wave height (H_{RMS});
f_w a friction coefficient that is based on the Swart (1974) formulations and a roughness height of 1 mm;
ρ_w the density of the water.

2.6 Sediment transport model

The D-Water Quality process library is used to compute the mud dynamics. There is a time-step-based online coupling between the D-Flow FM and the D-Water Quality modules, such that the hydrodynamics and sediment dynamics are computed in parallel.

2.6.1 The buffer model

The buffer model that was originally introduced by Van Kessel et al. (2011) is adopted for the exchange of mud between the bed and the water column. This model schematizes the seabed into two layers (Figure 2.8). The first layer (S1) is representative for the thin fluff layer on the bed surface. This layer is easily resuspended by (tidal) currents. The second layer (S2) is representative for the sandy seabed into which fines may entrain and temporarily be stored. Resuspension from this buffer layer is only significant during highly dynamic conditions, such as spring tide or storms.

Resuspension from the fluff layer (E1) and from the buffer layer (E2) are determined based on the resuspension parameter M and the dimensionless excess bed shear stress:

$$E_1 = m_1 M_1(\tau/\tau_{cr,S1} - 1) \quad \text{if} \quad m_1 \le M_0/M_1$$
$$E_1 = M_0(\tau/\tau_{cr,S1} - 1) \quad \text{if} \quad m_1 > M_0/M_1$$
$$E_2 = p_2 M_2(\tau/\tau_{cr,S2} - 1)^{1.5}$$

in which $\tau_{cr,Si}$ is the critical shear stress for erosion for layer i ($\tau_{cr,S1} < \tau_{cr,S2}$), M_0 the zeroth order resuspension parameter for layer S1, M_1 the first order resuspension parameter for layer S1, M_2 the resuspension parameter for layer S2, m_1 the sediment mass per unit area in layer S1 and p_2 the fines fraction in layer S2.
The deposition to the fluff layer (D1) and to the buffer layer (D2) are determined as:

$$D_1 = \beta(1-\alpha)w_s C$$
$$D_2 = \beta\alpha w_s C$$

in which w_s is the settling velocity, C the near-bed sediment concentration, β the deposition efficiency and α the fraction of the deposition flux to layer S2.

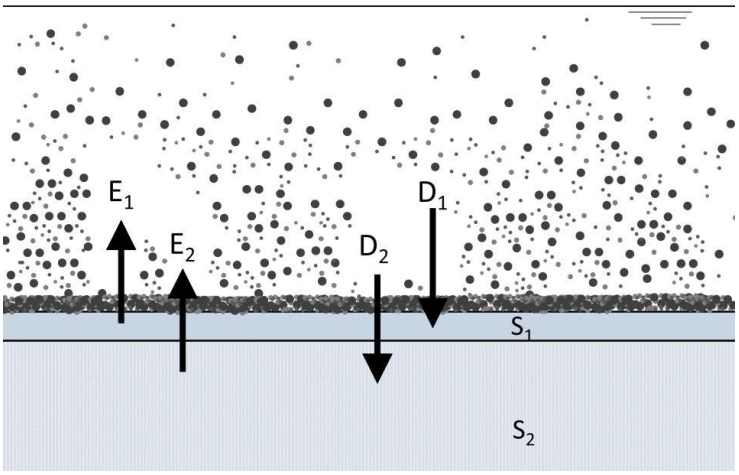

Figure 2.8 Schematic representation of the buffer model, with S1 a thin fluff layer and S2 the sandy seabed into which fines may infiltrate. E1 and E2 are the resuspension fluxes from layers S1 and S2. D1 and D2 are the deposition fluxes to layers S1 and S2.

2.6.2 Sediment properties and transport settings

The sediment transport settings are adopted from an earlier version of the DWSM model (Vroom et al., 2020). These settings are determined by calibrating the model to reproduce spatially varying mean sediment concentrations, variations in sediment concentrations at different timescales (i.e. intra-tidal variations, seasonal variations and storm impact), vertical concentration profiles, and the spatial variation of mud in the seabed.

The sediment transport model includes two mud fractions that differ from each other in their settling velocity. The first mud fraction (IM1) represents macro flocs and the second mud fraction (IM2) represents micro flocs.

Table 2.1 Sediment properties and transport settings in DWSM-Mud, adopted from the calibration of an earlier version of the DWSM model by Vroom et al. (2020).

Sediment property	Value
Settling velocity (w_s)	1.5 mm/s for mud fraction IM1 0.4 mm/s for mud fraction IM2
Deposition efficiency (β)	0.25
Fraction of the deposition to layer S2 (α)	0.05
Critical shear stress for erosion for layer S1 ($\tau_{cr,S1}$)	0.1 Pa
0th order erosion parameter for layer S1 (M_0)	$6.9*10^{-6}$ kg/m^2/s
1st order erosion parameter for layer S1 (M_1)	$5.8*10^{-6}$ 1/s
Critical shear stress for erosion for layer S2 ($\tau_{cr,S2}$)	0.8 Pa
Erosion parameter for layer S2 (M_2)	$1.5*10^{-4}$ kg/m^2/s
Thickness of layer S2	0.1 m

2.7 Open boundary conditions

2.7.1 Hydrodynamic boundary conditions

At the southern, western, northern, and eastern sides of the model domain, open boundaries are defined. The eastern boundary is split in two separate parts: one to the north and the other to the south of the German Wadden island of Baltrum. Boundary conditions are specified at in total 305 different support points along those boundaries. In between these locations the imposed values are interpolated linearly.

At the open boundary support points water levels, advective velocities, salinities and temperatures are prescribed with a 10-minute temporal interval. The values of the prescribed quantities are derived by off-line nesting in the 2022 release of 3D DCSM-FM model (Zijl et al., 2022b). The spatial resolution of the support points is as high as the network resolution of this model, which implies that hardly any information is lost in the spatial interpolation during nesting.

During test computations as part of the initial development of this model it was found that the prescription of advective velocity boundaries has a minor effect on the computed water levels. However, it leads to less disturbances in velocity fields near the open boundaries and may improve transport. It was therefore decided to make use of advective velocity boundaries in DWSM.

While the 2022 release of 3D DCSM-FM, from which the DWSM open boundary conditions are obtained, uses 50 z-sigma layers, only the upper 20 sigma layers are active at the location of the DWSM open boundaries. Therefore, salinity and temperature are prescribed at 20 sigma levels and internally interpolated by the D-Flow FM to the vertical model layers used by DWSM (i.e., 10 sigma layers).

2.7.2 Mud concentrations at the open boundaries

The depth-averaged mud concentrations that are imposed at the open boundaries follow a seasonal variation and are depending on the water depth at the boundary support points. Both the seasonal variation and the depth-dependency of the mud concentrations are based on the analysis of MWTL measurements in the Dutch coastal system by Herman et al. (2018). It was found in this analysis that the time-averaged mud concentration at observation points in the North Sea after natural log-transformation depends linearly on the logarithm of the depth of the water column, as was also described by Eleveld et al. (2008). The seasonal variation in the mud concentrations is imposed by a sine wave around the mean concentrations, such that the concentration in winter is about twice as high as the concentration in summer.

The total sediment concentration at the open model boundaries is distributed evenly over the two sediment fractions.

With these boundary conditions, the longshore transport of mud along the Dutch coast is in the order of 10 million tonnes per year. This is well aligned with estimates of the mud transport along the Dutch coast in literature, although Herman et al (2018) estimate the residual mud transport to be slightly higher, in the order of 20 million tonnes per year.

2.8 Meteorological forcing

DWSM has been coupled to ECMWF's ERA5 reanalysis dataset, which has a 0.25 degrees (~30 km) spatial resolution and hourly temporal resolution. The forcing parameters used are described below.

2.8.1 Momentum flux

To account for the air-sea momentum flux, time- and space-varying neutral wind speeds (at 10 m height) and atmospheric pressure (at MSL) are applied. With respect to air-sea momentum exchange, the aim is to be consistent with the Atmospheric Boundary Layer (ABL) model that is used in the meteorological model applied. For coupling to ERA5 this implies using a Charnock formulation (Charnock, 1955) and specifying a time-and space-varying Charnock coefficient. The Charnock formulation assumes a fully developed turbulent boundary layer of the wind flow over the water surface. The associated wind speed profile follows a logarithmic shape.

Air density

The air-sea momentum exchange is proportional to the air density. While in reality the air density varies in time and space, this quantity is taken to be constant in the wind drag formulations available in D-Flow FM. Therefore, the neutral wind speed as taken from ERA5 has been adjusted in a pseudo-wind approach. This implies that the wind speed was adjusted such that the resulting wind stress using a constant air density would be the same as the wind stress when using the original neutral wind speed in combination with a time-and space-varying air density. The air density was computed based on the ERA5 quantities atmospheric pressure, air temperature and dew point temperature.

Relative wind effect

In many wind-drag formulations the flow velocity at the water surface is not taken into account in determining the wind shear stress (i.e., the water is assumed to be stagnant). Even though the assumption of a stagnant water surface is common because it makes computing stresses easier, from a physical perspective the use of relative wind speed makes more sense since all physical laws deal with relative changes. In case the flow of water is in opposite direction to the wind speed, this would contribute to higher wind stresses (and vice-versa). The impact of the water velocity on the wind stress at the surface, and consequently also on computed water levels, is indicated with the name ‘Relative Wind Effect’ (RWE).

In general, including RWE leads to a meaningful improvement in (skew) surge quality during calm conditions (Appendix C of Zijl & Groenenboom, 2019; Zijl, 2021; Groenenboom & Zijl, 2021). Apparently, RWE adds an effect that cannot be fully incorporated by adjusting the bottom roughness instead. In this 2022 release an additional factor has been introduced to account for the fact that the wind speeds applied are not taken from a two-way coupled ocean–atmosphere system. In a two-way coupled system, the lowest layers of air would tend to move along with surface currents, reducing the relative wind effect. Following e.g. Lellouche et al. (2018) we therefore pragmatically consider a reduction of the model currents in the wind stress computation of 50%.

2.8.2 Heat-flux

Horizontal and vertical spatial differences in water temperature affect the transport of water through its impact on the water density. For example, heating of surface water and shallow waters causes temperature gradients that can generate horizontal flow. It can also lead to temperature stratification with accompanying damping of turbulence and hence a reduction in vertical mixing. To include these effects, the transport of temperature is modelled. For its main driver, exchange of heat between the water surface and the atmosphere, a heat-flux model is used. This model considers the separate effects of solar (shortwave) and atmospheric (longwave) radiation, as well as heat loss due to back radiation, evaporation and convection.

The temporally and spatially varying turbulent exchange of heat through the air-water interface, due to evaporation and convection, is computed based on the local temperature (at 2 m above the water surface), dew point temperature (also at 2 m) and wind speed (at 10 m) from the

ERA5 meteorological reanalysis. The Stanton and Dalton coefficients for parametrizing respectively the convective and the evaporative heat fluxes are both set to $1.3 * 10^{-3}$.
Usually, the evaporative heat flux transfers heat for water to air. However, in some circumstances condensation occurs, which implies a change in direction of this flux. Tests have shown that allowing this contributes to an improved representation of sea surface temperature. This is implemented in the final model version and achieved by setting the keyword *jadelvappos=0*.

To account for the radiative heat fluxes the surface net solar (short-wave) radiation and the surface downwelling long wave radiation have been imposed, while the surface upwelling long-wave radiation is computed based on the modelled sea surface temperature. The incoming solar radiation is distributed over the water column, depending on the water transparency prescribed with a Secchi depth. In the North Sea part of the domain a value of 4 m has been applied, while in the Wadden Sea this value is set to 1 m, reflecting enhanced concentrations of, for example, suspended sediment.

No buffering of heat in the soil is included in this model (*Soiltempthick=0*).

2.8.3 Mass-flux

To account for the mass-flux through the air-sea interface time- and space varying fields of evaporation and precipitation have been applied.

2.9 Freshwater discharges

Freshwater discharges in the DWSM domain are prescribed as sources based on measured timeseries of the discharge. The largest and therefore the most important freshwater sluices for the hydrodynamics are the sluices in the Afsluitdijk (near Den Oever and Kornwerderzand) and the Cleveringsluizen in the Lauwersmeer. Other freshwater sluices that are included in the model are located along the mainland coast. The locations are shown in Figure 2.9. The freshwater discharge from the Ems river is also included as a freshwater source, based on measured discharges at Herbrum and Leer. Table 2.2 lists the source of the data for each of the sources, as well as the temporal resolution of timeseries. The total discharge in 2017 of each of the freshwater sources that are included in the model is shown in Figure 2.10.

The salinity of all discharged water is assumed to be 0.2 psu. The temperature of discharged water is based on nearby measurements of surface water temperature (see Table 2.2).

The mud concentrations in the discharged water are set to 10 mg/L for each of the two mud fractions. The total mud concentration of 20 mg/L is based on a multi-year averaged concentration in MWTL measurements. The mud concentration in the discharged water is schematized to be constant in time, such that temporal variations in the total mud discharge are only due to variations in the discharge of water. The total amount of mud that is brought into the model via the freshwater discharges in 2017 is around 0.4 million tonnes.

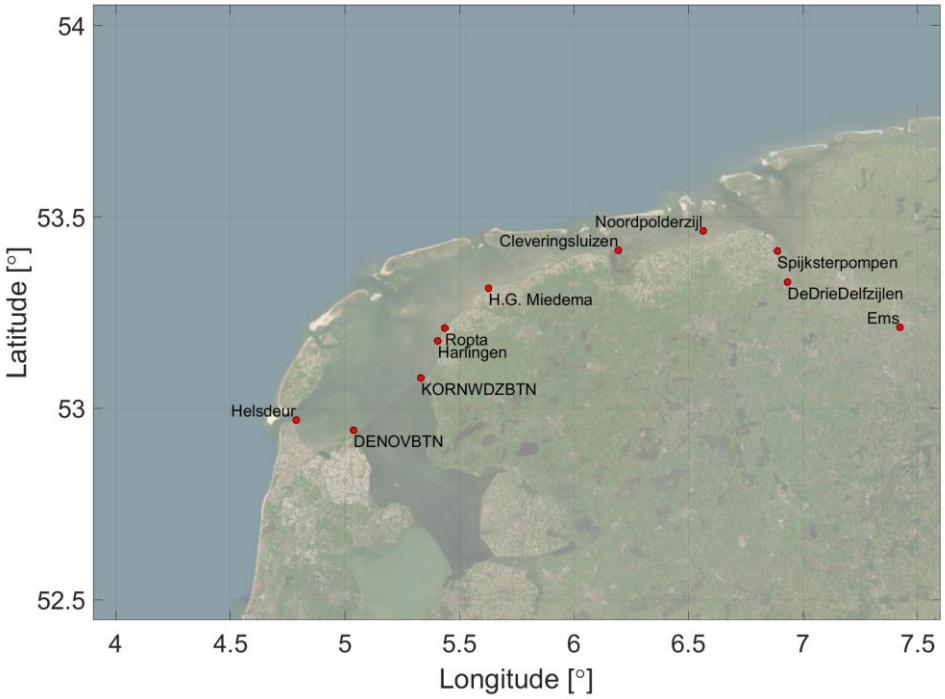

Figure 2.9 Location of freshwater discharges that are included as sources in the DWSM domain.

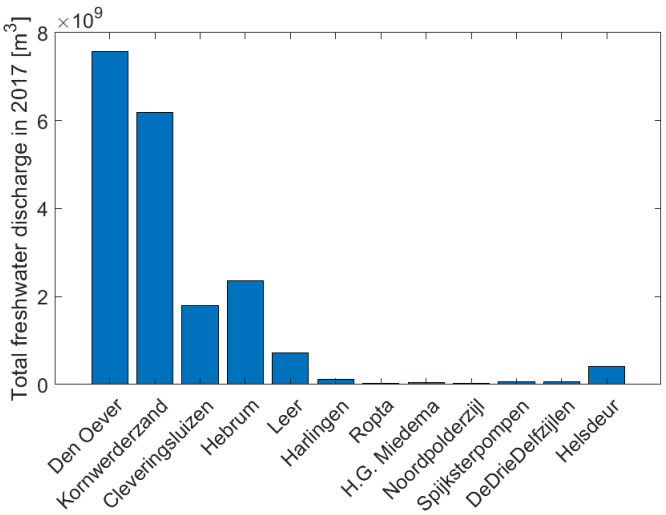

Figure 2.10 Cumulative discharge of each of the freshwater sources in 2017.

Table 2.2 List of freshwater discharges included in DWSM as sources, with temporal resolution, data source and location used for associated water temperature.

Location	Temporal resolution	Data source	Location used for water temperature
Den Oever	10 min	Rijkswaterstaat (Matroos database)	Den Oever
Kornwerderzand	10 min	Rijkswaterstaat	Kornwerderzand buiten
Cleveringsluizen	15 min	Noorderzijlvest	Schiermonnikoog
Ems (Herbrum)	1 day	Datahuis Wadden	Schiermonnikoog
Ems (Leer)	1 month	Datahuis Wadden	Schiermonnikoog
Harlingen	1 day	Datahuis Wadden	Schiermonnikoog
Ropta	1 day	Datahuis Wadden	Schiermonnikoog
H.G. Miedema	1 day	Datahuis Wadden	Schiermonnikoog
Noordpolderzijl	1 day	Waterschap Noorderzijlvest	Schiermonnikoog
Spijksterpompen	15 min	Waterschap Noorderzijlvest	Schiermonnikoog
DeDrieDelfzijlen	15 min	Waterschap Noorderzijlvest	Schiermonnikoog
Helsdeur	15 min	Hoogheemraadschap Hollands Noorderkwartier (based on operational forecasting)	Schiermonnikoog

2.10 Numerical settings

2.10.1 Time step

D-Flow FM automatically limits the time step to prevent numerical instabilities. Since the computation of the advective term is done explicitly in D-Flow FM, the time step limitation is related to the Courant criterion. In accordance with Minns et al. (2022) the maximum Courant number is set to 0.7. The maximum computational time step has been set to 100 s.

The time step for D-Water Quality processes is set equal to the hydrodynamic time step.

2.10.2 Differences with sixth-generation standard settings

While most geometric, numerical and physical model settings of DWSM are in accordance with the current specifications for sixth-generation models as described in Minns et al. (2022), there are some settings that deviate from the standard. These keywords and settings are listed in Table 2.3 for the 2D keywords, in
Table 2.4 for keywords associated with exchange with the atmosphere and in Table 2.5 for 3D keywords.

Table 2.3 Overview of 2D keywords where settings of DWSM differ from the standard settings.

Keyword	Standard setting	DWSM 2022 release
Dxwuimin2D	0	0.1
BedlevUni	-5	5
OpenBoundaryTolerance	3	0.1
Izbndpos	0	1
Tlfsmo	0	86400
Rhomean	1000	1023
DtUser	300	600
DtMax	30	100
DtInit	1	30

Table 2.4 Overview of keywords associated with exchange with the atmosphere where settings of DWSM differ from the standard settings.

Keyword	Standard setting	DWSM 2022 release
Secchi depth	2	4 (1 in Waddenzee)
Stanton	-1	0.0013
Dalton	-1	0.0013
ICdtyp	2 (Smith & Banke)	4 (Charnock)
Relativewind	0	0.5
Rhoair	1.205	1.2265
Soiltempthick	1	0
RhoairRhowater	0	1
Jadelvappos	1	0

Table 2.5 Overview of 3D keywords where settings of DWSM differ from the standard settings.

Keyword	Standard setting	DWSM 2022 release
vicoww	5E-5	1.0E-4
dicoww	5E-5	1.4E-5

2.11 Miscellaneous

2.11.1 Tidal potential

In DCSM-FM 100m, from which the 2D settings of DWSM are taken, the tidal potential representing the direct body force of the gravitational attraction of the moon and sun on the mass of water has been switched on. The effect of this decreases with decreasing model extent. Since the impact of the tidal potential is expected to be limited on the scale of the Wadden Sea, this option has been switched off in DWSM.

2.11.2 Horizontal turbulence

The horizontal viscosity is computed with the Smagorinsky sub-grid model, with the coefficient set to 0.20. The use of a Smagorinsky model implies that the viscosity varies in time and space and is dependent on the local cell size. In addition, a background value of 0.1 m^2/s is specified.

2.11.3 Vertical turbulence

A k-ε turbulence closure model is used to compute the vertical eddy viscosity and diffusivity. In addition, a background value of 1.0 x 10^{-4} m^2/s is set for vertical eddy viscosity, which is a commonly used value to account for vertical transfer of momentum due to the presence of internal waves. For vertical eddy diffusivity, a background value of 1.4 x 10^{-5} m^2/s is used. This value has been determined after doing sensitivity simulations, comparing the modelled and measured vertical temperature difference (a measure of temperature stratification) at a location in the central North Sea.

2.11.4 Initial conditions and spin-up period

The model starts from a dynamic equilibrium on 22 December 2016, which consists of spatially varying fields for the hydrodynamics, temperature, salinity, mud concentrations and the amount of mud in the bed.

The dynamic equilibrium for hydrodynamics, temperature and salinity is the result of a spin-up simulation of one year. A uniform initial water level of zero elevation has been specified for the spin-up computations, while for the initial velocity, stagnant flow conditions have been prescribed. Salinity and temperature are initialized with a value that reflects average conditions along the open boundaries at the start of the computation (34.17 psu and 9.55 °C).

The dynamic equilibrium for mud concentrations and the amount of mud in the bed is the result of a series of spin-up simulations with a total duration of three years. The initial sediment distribution in layer S2 in the first spin-up simulation is based on measurements of the mud fraction in the seabed, using the Sediment Atlas of the Wadden Sea (Rijkswatersaat, 1998). It is assumed that the total amount of mud in the bed consists for 80% out of mud fraction IM1 and for 20% out of mud fraction IM2, as fraction IM2 has a lower settling velocity and will therefore be more likely to stay in suspension than fraction IM1. The sediment distribution in the bed reached a dynamic equilibrium after a spin-up period of three years; an additional year of spin-up did not anymore lead to significant differences in the sediment distribution in the bed. The dynamic equilibrium for the sediment distribution is discussed as part of Section 4.5.

2.11.5 Time zone

The time zone of DWSM is GMT+0 hr. This means that the boundary conditions and meteorological forcing are prescribed relative to GMT+0 hr. As a result, the model output is in the same time zone.

2.11.6 Observation points

At 110 stations within the model domain timeseries are written of water levels, velocities, salinity, temperature, mud concentrations and other modelled parameters. The locations of these observation points are presented in Figure 2.11 and Figure 2.12. The main stations used in the validation of water levels (section 3.1.6), in the validation of salinity (section 3.5) and temperature (section 3.6), and in the validation of mud concentrations (chapter 4) are highlighted. If locations are just outside the model grid or if model results showed erroneous drying, they are manually placed in the closest cell with sufficient depth.

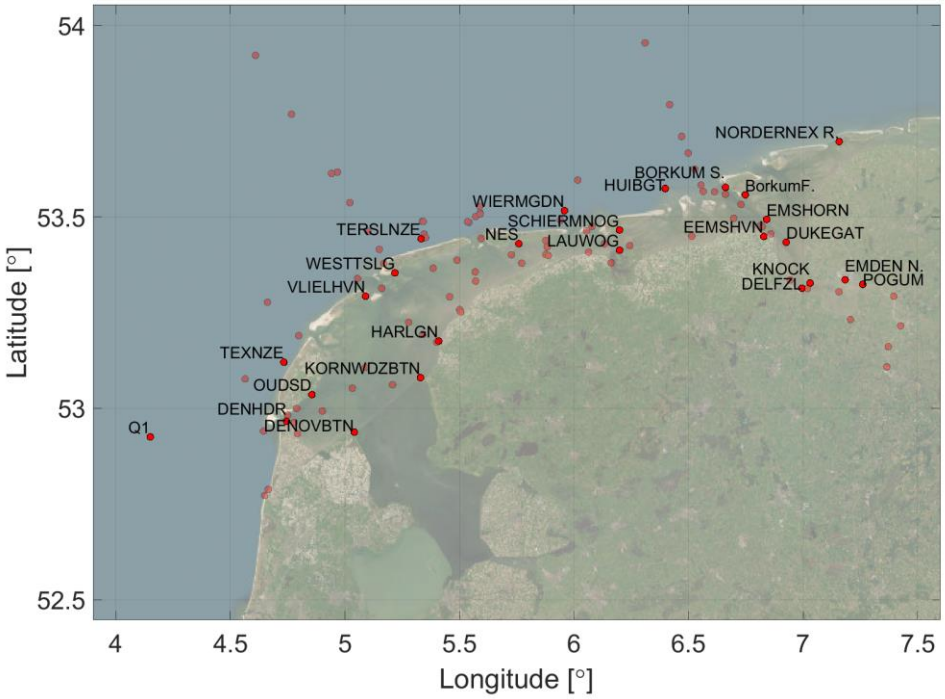

Figure 2.11 Location of observation points in DWSM with the main stations used for the water level validation highlighted.

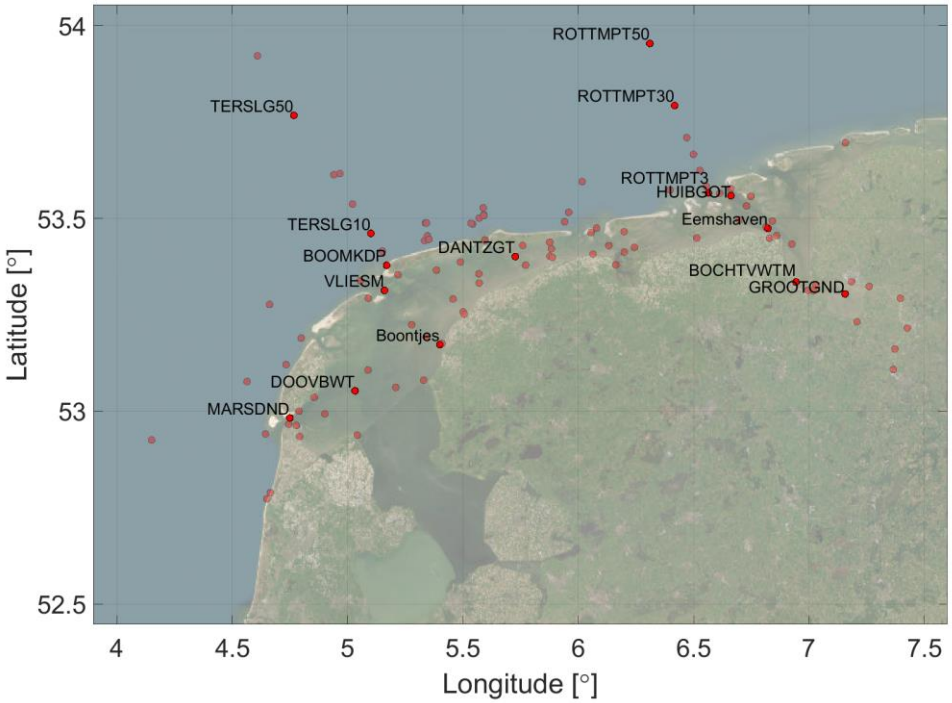

Figure 2.12 Location of observation points in DWSM with the main stations used for the validation of salinity, temperature and mud concentrations highlighted.

2.11.7 Software version

DWSM has been developed as an application of the D-Flow Flexible Mesh module (D-Flow FM) of the D-HYDRO Suite. This module is suitable for one-, two-, and three-dimensional hydrodynamic modelling of free surface flows on unstructured grids. Various versions of D-Flow FM have been used during the development of DWSM. For the validation of the DWSM hydrodynamic model that is presented in this report, use has been made of D-Flow FM version

1.2.173.142106 (December 1, 2022). For the validation of the mud model (DWSM-Mud) that is presented in this report, use has been made of DIMRset 2.26.16 (D-Flow FM version 1.2.184.39524a25ec694191c157602a672a0246cd6e004a; February 26, 2024). Although a slightly older software version has been used during the validation, DWSM-Mud is released for public use with D-HYDRO Suite version 2024.03.

2.11.8 Computational time

Computations are performed on Deltares' h6 Linux-cluster (queue: codec) using 5 nodes with 4 cores each. With a maximum timestep of 100 s, and an average timestep of 57.2 s, this results in a computational time of the hydrodynamic DWSM model of 6.4 minutes per simulation-day (1.6 days per simulation-year). The computational time of the combined hydrodynamic and mud model is 11.6 minutes per simulation-day (2.9 days per simulation-year).

3 Validation – Hydrodynamics

3.1 Water levels

3.1.1 Introduction

DWSM is validated against tide gauge measurements for the entire year of 2017. This period coincides with the year for which the bottom roughness that was obtained from DCSM-FM 100m was calibrated. The validation results are presented in this chapter.

3.1.2 Model comparison

In this chapter, validation results are compared to other numerical models. The three models of interest for comparison are:

- 3D DCSM-FM 0.5nm (2022 release)
- DCSM-FM 100m (2022 release)
- DWSM (first release)

3D DCSM-FM uses the same meteorological forcing as DWSM (ECMWF ERA5), while for DCSM-FM 100m the higher resolution ECMWF IFS meteorological forcing is used. For the first release of DWSM Hirlam meteorological forcing was used.

3.1.3 Quantitative evaluation measures (Goodness-of-Fit parameters)

Total water level, tide and surge

To assess the quality of the computed water levels, the root-mean-square error (RMSE) is computed based on measured and computed total water levels for the entire validation period (the year 2017). In addition, as it provides further insight in the origins of remaining errors, the tide and surge component are separated from the total water level (see section 3.1.4) and the quality of both tide and surge is assessed separately.

Mean water level

In the present report, the bias between measured and computed water levels in each station, determined over the entire one-year validation period, is disregarded in the Goodness-of-Fit criteria used for total water levels, tide and surge. This is achieved by correcting the measurements for this bias before these criteria are determined. Consequently, when considering the entire period, the Root-Mean-Square (RMS) of the error signal is equal to the standard deviation thereof. An advantage of this approach is that it removes the need to convert all measurements to a uniform vertical reference plane that is valid for the entire model domain. At the Dutch NAP-referenced water level measurements the bias between modelled and measured water levels is separately presented.

3.1.4 Harmonic analysis

The separation of the tide and surge contribution to the total water level is done by means of harmonic analysis using the MATLAB package t_tide (Pawlowicz et al., 2002). After obtaining the tide through harmonic analysis and prediction, the surge (or ‘non-tidal residual’) is obtained by subtracting the predicted tide from the total water level signal. Harmonic analysis is only performed when the completeness index of the measurements is larger than 80% and the length of the available measurements within the analysis period is larger than 300 days. Based on the possibility to separate constituents using a time series of one year, 118 constituents have been selected to be used in the harmonic analysis.

3.1.5 Observation stations

For further analysis of the results, the emphasis will be on a set of 17 Dutch and eight German stations. A list of these 25 stations is presented in Table 4.3, in order of increasing M2 phase lag (i.e., in general from west to east).

Table 3.1 Station name and source of the tide gauge measurements used for quantitative model evaluation of DWSM.

Station	Source	Station	Source
Platform Q1	RWS	Lauwersoog	RWS
Den Helder	RWS	Schiermonnikoog	RWS
Texel Noordzee	RWS	Borkum Sudstrand	WSV[1]
Oudeschild	RWS	Borkum Fischerbalje	WSV[1]
Den Oever buiten	RWS	Emshorn	WSV[1]
Terschelling Noordzee	RWS	Eemshaven	RWS
Vlielandhaven	RWS	Norderney Riffgat	WSV[1]
West Terschelling	RWS	Dukegat	WSV[1]
Kornwerderzand buiten	RWS	Delfzijl	RWS
Wierumergronden	RWS	Knock	WSV[1]
Harlingen	RWS	Emden NeueSeeschleuse	WSV[1]
Huibertgat	RWS	Pogum	WSV[1]
Nes	RWS		

[1] *German Federal Waterways and Shipping Administration (WSV), communicated by the German Federal Institute of Hydrology (BfG).*

3.1.6 Total water levels, tide and surge

A spatial overview of the RMSE-values of the total water level, tide and surge is presented in Figure 3.1, Figure 3.2 and Figure 3.3, respectively. The underlying values are also presented in Table 3.2, which also contains the statistics from DCSM-FM 100m – the model from which the bottom roughness is taken - and 3D DCSM-FM, from which the open boundary conditions are derived.

These results show that total water levels errors are generally between 5-8 cm, with the lowest errors in the North Sea stations. The tidal error is generally between 4-5 cm. Exceptions are Den Oever buiten and West-Terschelling with tidal errors of around 9 cm. Upstream in the Ems-Dollard, in Emden and Pogum, the tidal error increases to 12 cm and 19 cm, respectively. In these areas the model resolution is relatively low compared to the variability in geometry and bathymetry. This results in a poorer representation of the tide, also compared to the higher resolution DCSM-FM 100m model.

The surge error generally varies between 4-6 cm, with the lowest in the North Sea and increasing towards the mainland coast and upstream the Ems-Dollard.

Compared to 3D DCSM-FM, the tide quality of DWSM is equal or better in most stations. The only stations that deteriorate by more than 0.5 cm are Oudeschild, Den Oever buiten, West-Terschelling, Kornwerderzand; all located in the western Wadden Sea. Since the boundary conditions are obtained from 3D DCSM-FM this might be either due to a poor local

representation of geometry or bathymetry, or due to a bottom roughness that is inconsistent with the boundary conditions.
The surge quality is generally equal or better than in 3D DCSM-FM. Since both the boundary conditions are obtained from 3D DCSM-FM and the surface forcing is the same in both models, the improvements are probably due to a better representation of local bathymetry in the finer DWSM network.

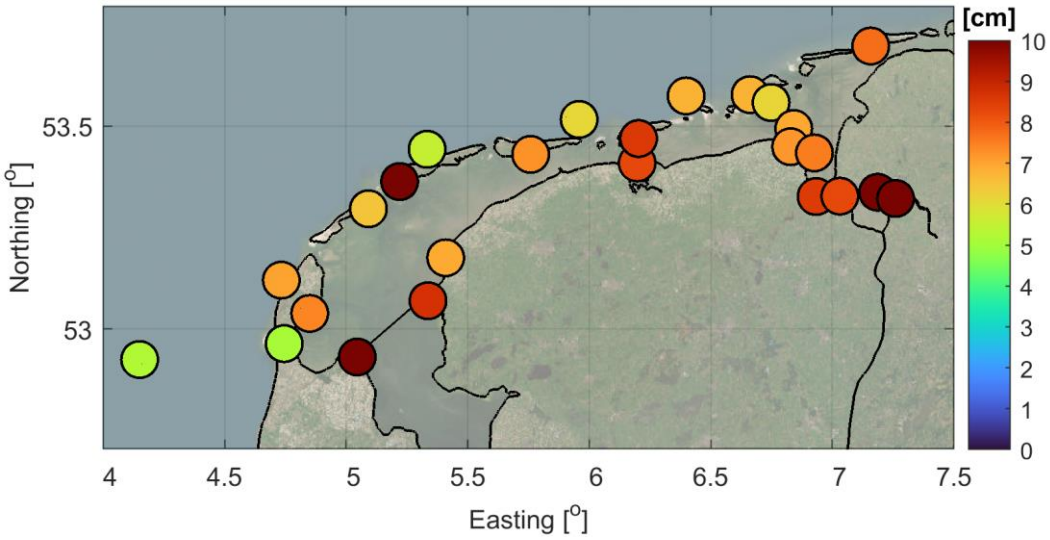

Figure 3.1 Spatial overview of the total water level RMSE (cm) for the validation year 2017.

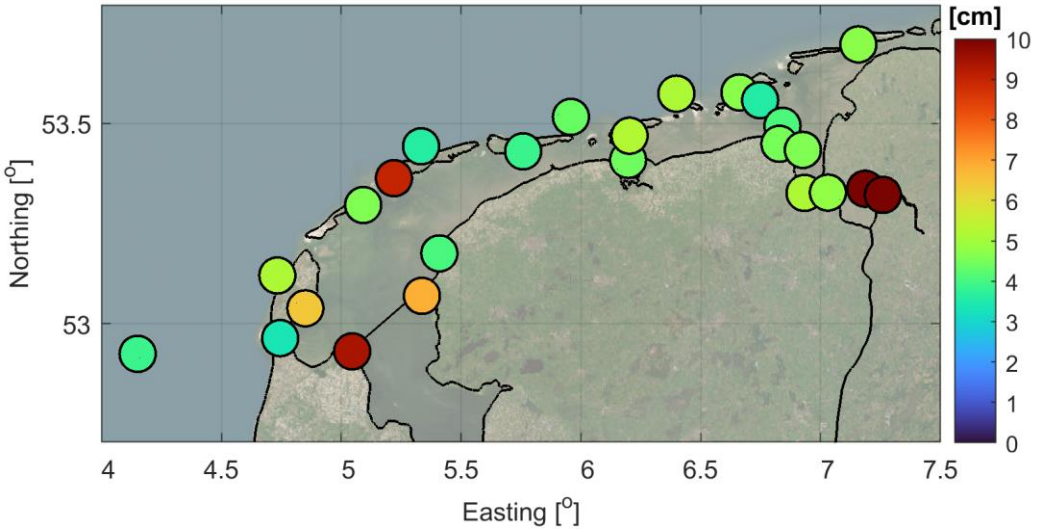

Figure 3.2 Spatial overview of the tide RMSE (cm) for the validation year 2017.

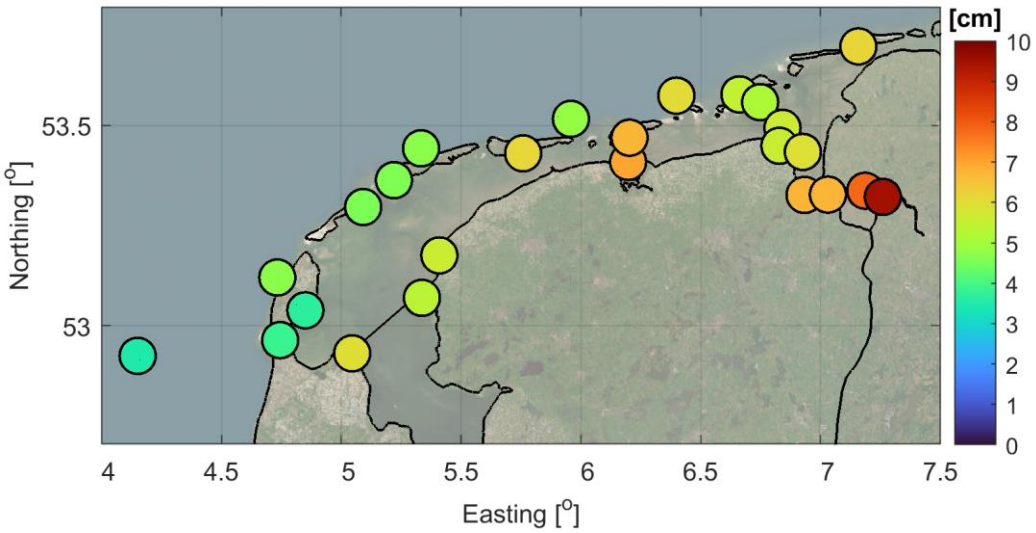

Figure 3.3 Spatial overview of the surge RMSE (cm) for the validation year 2017.

Table 3.2 Statistics (RMSE in cm) of tide, surge and total water level of 3D DCSM-FM, DCSM-FM and DWSM. DCSM-FM 100m used meteorological forcing from the operational product of ECMWF. 3D DCSM-FM and DWSM use ERA5.

Station	RMSE tide (cm)			RMSE surge (cm)			RMSE water level (cm)		
	3D DCSM-FM	DCSM-FM 100m	DWSM	3D DCSM-FM	DCSM-FM 100m	DWSM	3D DCSM-FM	DCSM-FM 100m	DWSM
Q1	4.0	3.0	3.9	3.5	3.9	3.5	5.3	4.9	5.2
DENHDR	3.0	3.5	3.4	3.9	4.2	3.8	4.9	5.4	5.1
TEXNZE	5.6	5.1	5.2	4.8	5.0	4.7	7.4	7.1	7.0
OUDSD	3.1	3.8	6.4	3.7	4.0	3.7	4.8	5.5	7.4
DENOVBTN	3.9	6.1	9.4	6.3	5.3	6.0	7.5	8.1	11.1
TERSLNZE	3.6	4.3	3.6	4.7	5.0	4.7	5.5	6.2	5.5
VLIELHVN	12.4	5.2	4.6	7.0	4.4	4.6	14.3	6.8	6.5
WESTTSLG	5.2	6.4	9.0	5.0	4.6	4.6	7.2	7.9	10.1
KORNWDZBTN	4.4	3.7	6.8	5.1	4.9	5.4	6.7	6.1	8.7
WIERMGDN	4.3	4.2	4.4	4.8	5.0	4.8	6.0	6.1	6.1
HARLGN	4.9	4.8	4.0	6.0	5.4	5.6	7.8	7.3	6.9
HUIBGT	4.8	5.3	5.2	5.9	6.2	6.0	6.5	7.0	6.8
NES	11.8	4.7	3.9	7.8	6.1	6.1	14.2	7.7	7.2
LAUWOG	6.8	5.6	4.5	7.4	6.8	7.0	10.1	8.8	8.3
SCHIERMNOG	16.2	4.8	5.3	9.8	6.4	6.7	18.9	8.0	8.5
BORKUM_Sudstrand	5.4	5.3	4.7	5.4	5.7	5.5	7.3	7.3	6.8
BorkumFischerbalje	6.5	4.1	3.6	4.9	5.3	5.2	8.0	6.6	6.1
EMSHORN	4.5	5.2	4.1	5.6	5.8	5.6	7.2	7.8	6.9
EEMSHVN	6.4	4.9	4.5	5.5	5.7	5.6	8.4	7.5	7.2
NORDERNEX_RIFFG		6.5	4.7		6.3	6.1		9.0	7.7
DUKEGAT	5.6	4.8	4.6	5.9	5.9	5.9	8.1	7.6	7.5

Station	RMSE tide (cm)			RMSE surge (cm)			RMSE water level (cm)		
	3D DCSM-FM	DCSM-FM 100m	DWSM	3D DCSM-FM	DCSM-FM 100m	DWSM	3D DCSM-FM	DCSM-FM 100m	DWSM
DELFZL	7.0	5.5	5.2	7.1	6.8	6.7	10.0	8.8	8.5
KNOCK	6.5	5.6	4.8	7.0	6.8	6.7	9.6	8.8	8.3
EMDEN_Neue_Seeschl		7.6	12.3		7.3	7.8		10.5	14.6
POGUM		9.3	19.2		8.0	9.5		12.2	21.4
Average (total)	**6.2**	**5.2**	**5.9**	**5.8**	**5.6**	**5.7**	**8.4**	**7.6**	**8.2**

Comparison to the first DWSM release

In Table 3.3, the statistics of tide, surge and total water level of the first and second release of DWSM are compared. Note that these models use a different meteorological forcing: Hirlam for the first release and ERA5 for the second release. Only stations that are present in both model versions have been included.

These results show that on average the model quality has improved for tide, surge and total water levels. With respect to tide, of the 22 stations considered, only four stations show a deterioration: Oudeschild, Den Oever buiten, West-Terschelling, Kornwerderzand. These are the same stations that perform considerably worse than 3D DCSM-FM. The surge improves in the stations in the western Wadden Sea, while in the eastern Wadden Sea, in particular the Ems-Dollard estuary, some stations deteriorate. This is probably related to the much coarser resolution of the meteorological forcing used in the second release (ERA5).

Some of the most notable improvements are present in tide gauge stations Harlingen and Schiermonnikoog, which were the poorest performing stations in the first release, due to a misrepresentation of low waters in particular. This is visualized with scatter plots of measured and modelled total water levels in Figure 3.6 (Harlingen) and Figure 3.5 (Schiermonnikoog), and shows a that in the second release of DWSM the low waters in these stations are well represented. The low water representation for tide gauge station Holwerd, presented in Figure 3.6, remains poor, due to the relatively coarse schematization of bathymetry, in relation to the width of the channel towards Holwerd.

Table 3.3 Statistics (RMSE in cm) of tide, surge and total water level of the first and second release of DWSM. The first release used meteorological forcing from Hirlam, while the second release makes use of ERA5.

Station	RMSE tide (cm)		RMSE surge (cm)		RMSE water level (cm)	
	DWSM 1st release	DWSM 2nd release	DWSM 1st release	DWSM 2nd release	DWSM 1st release	DWSM 2nd release
Q1	4.8	3.9	4.1	3.5	6.3	5.2
DENHDR	4.3	3.4	4.2	3.8	6.1	5.1
TEXNZE	6.1	5.2	5.2	4.7	8.0	7.0
OUDSD	4.3	6.4	4.2	3.7	6.0	7.4
DENOVBTN	4.3	9.4	6.6	6.0	7.9	11.1
TERSLNZE	4.8	3.6	5.2	4.7	6.5	5.5
VLIELHVN	6.4	4.6	5.0	4.6	8.2	6.5
WESTTSLG	5.7	9.0	4.8	4.6	7.4	10.1
KORNWDZBTN	4.4	6.8	5.6	5.4	7.1	8.7
WIERMGDN	5.2	4.4	5.4	4.8	6.9	6.1
HARLGN	9.1	4.0	9.3	5.6	13.0	6.9
HUIBGT	6.4	5.2	6.5	6.0	7.4	6.8

Station	RMSE tide (cm)		RMSE surge (cm)		RMSE water level (cm)	
	DWSM 1st release	DWSM 2nd release	DWSM 1st release	DWSM 2nd release	DWSM 1st release	DWSM 2nd release
NES	8.2	3.9	6.1	6.1	10.3	7.2
LAUWOG	5.9	4.5	6.7	7.0	8.9	8.3
SCHIERMNOG	23.0	5.3	12.4	6.7	26.1	8.5
BORKUM_Sudstrand	5.4	4.7	5.4	5.5	7.4	6.8
BorkumFischerbalje	6.5	3.6	6.7	5.2	9.2	6.1
EMSHORN	5.4	4.1	5.4	5.6	7.6	6.9
EEMSHVN	5.2	4.5	5.4	5.6	7.5	7.2
NORDERNEX_RIFFG	4.9	4.7	5.8	6.1	7.6	7.7
DUKEGAT	5.6	4.6	5.9	5.9	8.2	7.5
KNOCK	6.4	4.8	6.5	6.7	9.1	8.3
Average (total)	**6.5**	**5.0**	**6.0**	**5.4**	**8.8**	**7.3**

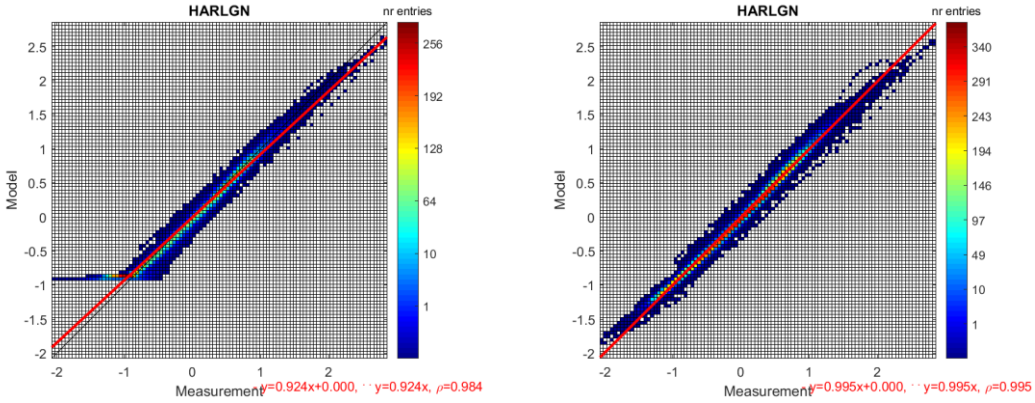

Figure 3.4 Scatterplots of measured and modelled total water levels for tide gauge station Harlingen, with the first release on the left and the second release on the right.

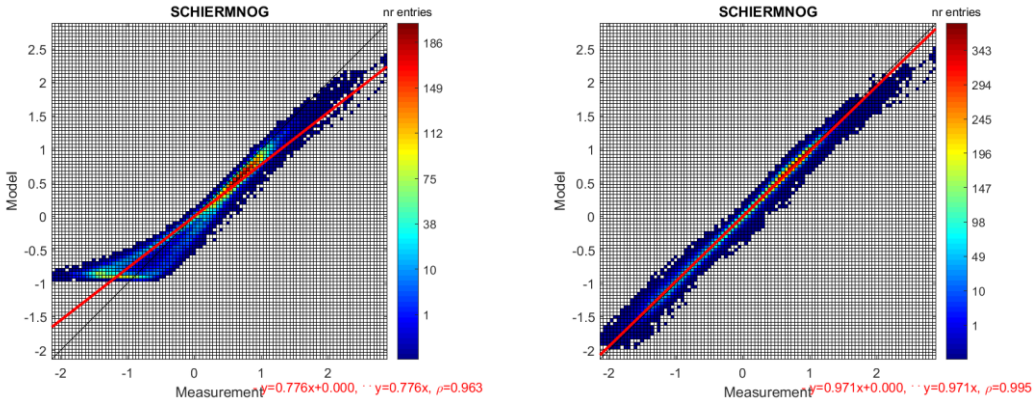

Figure 3.5 Scatterplots of measured and modelled total water levels for tide gauge station Schiermonnikoog, with the first release on the left and the second release on the right.

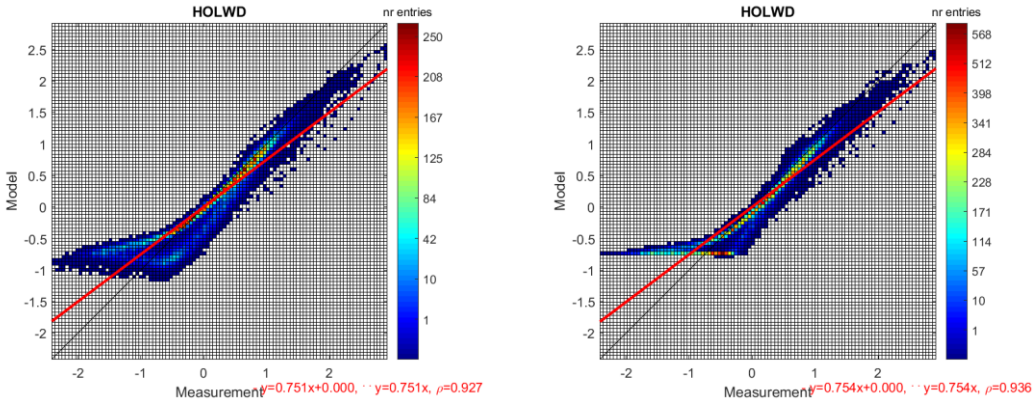

Figure 3.6 Scatterplots of measured and modelled total water levels for tide gauge station Holwerd, with the first release on the left and the second release on the right.

3.1.7 Bias in Dutch NAP-referenced stations

Figure 3.7 shows a spatial comparison of the bias between modelled and measured water levels. Station Delfzijl has been excluded, since the location of this station was adjusted from inside the harbour to just outside, which results in an unreliable bias. Further analysis of the underlying statistics shows a station-averaged bias of 1.7 cm and a standard deviation of bias between stations of 1.3 cm. This is an improvement upon the first release of DWSM, where the station-averaged bias was 8.5 cm and the standard deviation 3.5 cm.

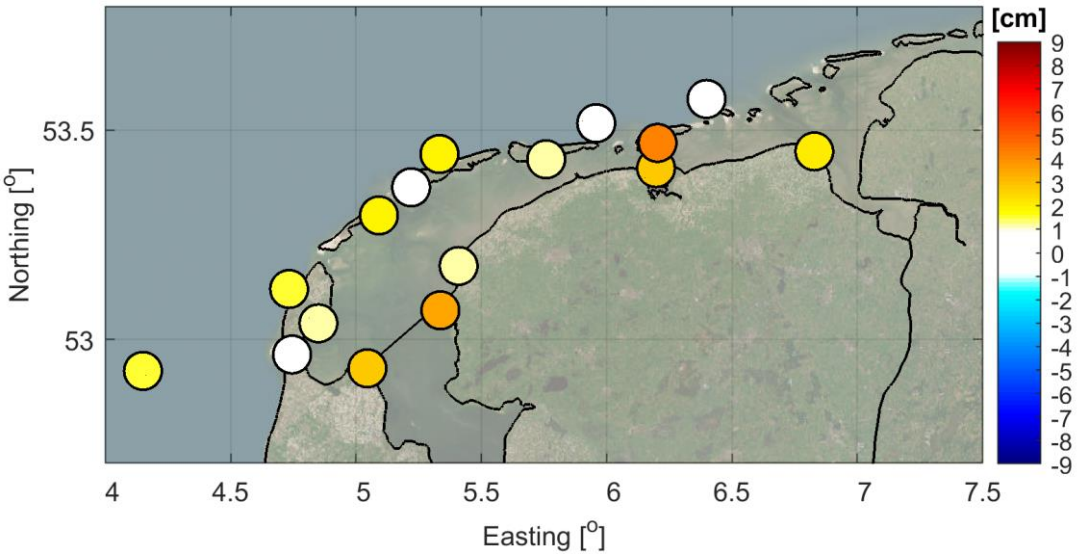

Figure 3.7 Spatial overview of bias between modelled and measured water levels in Dutch NAP-referenced stations.

3.1.8 Tide (frequency domain)

Figure 3.8 illustrates the amplitude and phase error of the M2-component, respectively. These results show that generally the amplitude error is at most 3 cm, while the phase error is at most 2°. The station-averaged M2 phase error is -1.4°, while the corresponding number for the M2 amplitude error is 1.2 cm.

Notable exceptions are four stations in the western Wadden Sea (Oudeschild, Den Oever buiten, West-Terschelling and Kornwerderzand), where large M2 phase errors occur of up to -8° and M2 amplitude error of up to 5 cm. This means that in the model, the tidal wave propagates faster and has a larger amplitude than in the observations. While the cause of these relatively large deviations from measurements are unknown, both are consistent with an underestimation of dissipation due to e.g. bottom friction. It is remarkable that the results for Harlingen are better, while this station is located further away from the inlet than the four stations mentioned above.

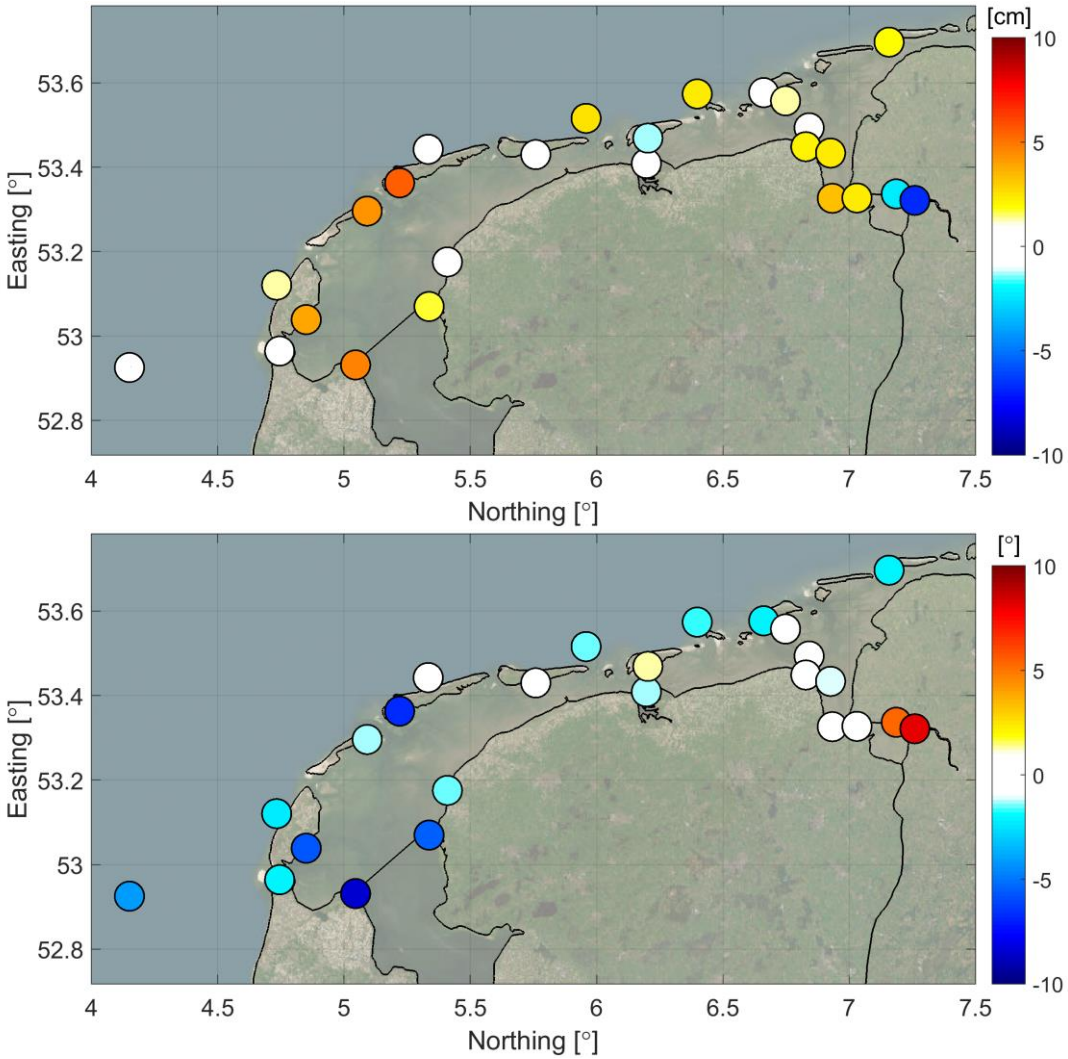

Figure 3.8 Spatial overview of the amplitude error (cm; top) and phase error (º; bottom) of the M2-component.

3.2 Currents

The reproduction of depth-averaged flow velocities by the model is validated by comparing the model results to observed flow velocities. During the Kustgenese 2.0 field campaigns around Ameland Inlet in 2017, flow velocities were measured by acoustic instruments. Observation points were located in the main channel of Ameland Inlet, at the ebb-tidal delta, at the lower foreshore and at the tidal divides of Terschelling and Ameland. The location of the observation points is shown in Figure 3.9. Van der Werf et al. (2019) contains a detailed description of the field campaigns and the processing of data. The measured flow velocity data used for the

comparison between model results and field data originates from depth-averaging after fitting a logarithmic velocity profile to the measured data.
In this section, the reproduction of depth-averaged flow velocities is illustrated for a few of the observation points. The ability of the model to reproduce the magnitude of the depth-averaged flow velocities is quantified for all the observation points in Table 3.4 and Table 3.5.

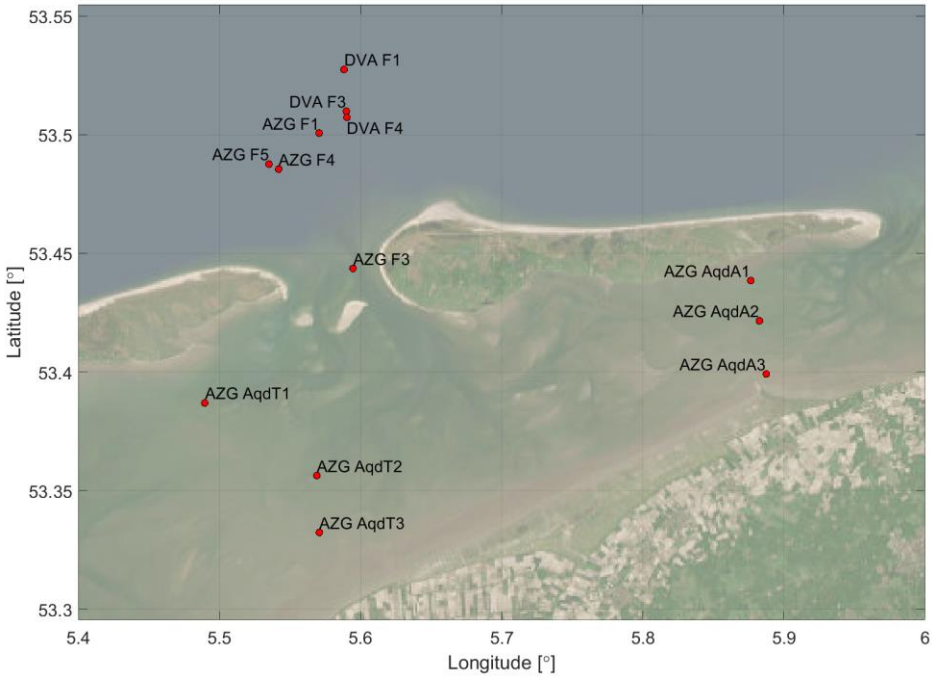

Figure 3.9 Measurement locations for flow velocities during the Kustgenese 2.0 field campaings in 2017.

Timeseries of the magnitude and direction of depth-averaged velocities at observation point DVA F1, located on the ebb-tidal delta, are illustrated in Figure 3.10. The RMSE of the flow magnitude for the period for which measurements are available (09/11/2017 – 11/12/2017) is 0.07 m/s (see also Table 3.4). This indicates that flow velocities in the model corresponds well with observations. The RMSE of the flow direction is approximately 25°, which is relatively large because of a bias in the flow direction. Further investigation of the model results indicates that the longshore flow velocities are reproduced much better (r = 0.99 for the west-east velocity component) than the cross-shore velocities (r = -0.18 for the south-north velocity component). Results are similar at observation points DVA F3 and DVA F4. This suggests that certain processes that cause a cross-shore current are not (well enough) included in the model. Waves (and in particular wave-driven currents) may be one of these, although the underestimation of the cross-shore flow also occurs during calm conditions, when the impact of waves on currents is expected to be more limited.

Observation points AZG-F4 and AZG-F5 are located in one of the channels of the ebb-tidal delta of Ameland Inlet. Therefore, the direction of the flow is largely aligned with the orientation of the channel. Figure 3.11 illustrates the timeseries at AZG-F4. Both the magnitude and the direction from model results are in good correspondence with the observations. During a storm on September 13th, the increase in flow velocities is captured, although the magnitude is underestimated by the model. Observations show a strong west-northwest oriented flow over the ebb-tidal delta during this storm, which is likely due to wave-effects that are not included in DWSM. The reproduction of the flow direction at AZG-F5 by the model is less good. This is possibly due to bathymetric changes between 2017 (i.e., at the time of flow measurements) and 2021 (i.e., when the bathymetric data that is used in the model bathymetry was collected).

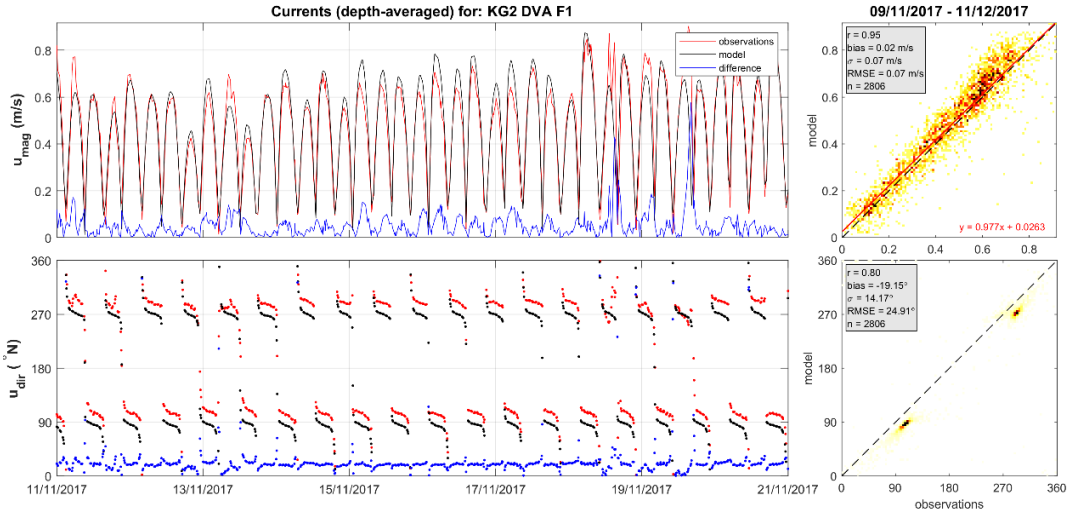

Figure 3.10 Timeseries of the magnitude (top) and direction (bottom) of depth-averaged flow velocities at observation point DVA F1 at the lower shoreface in observations (in red) and in model results (in black).

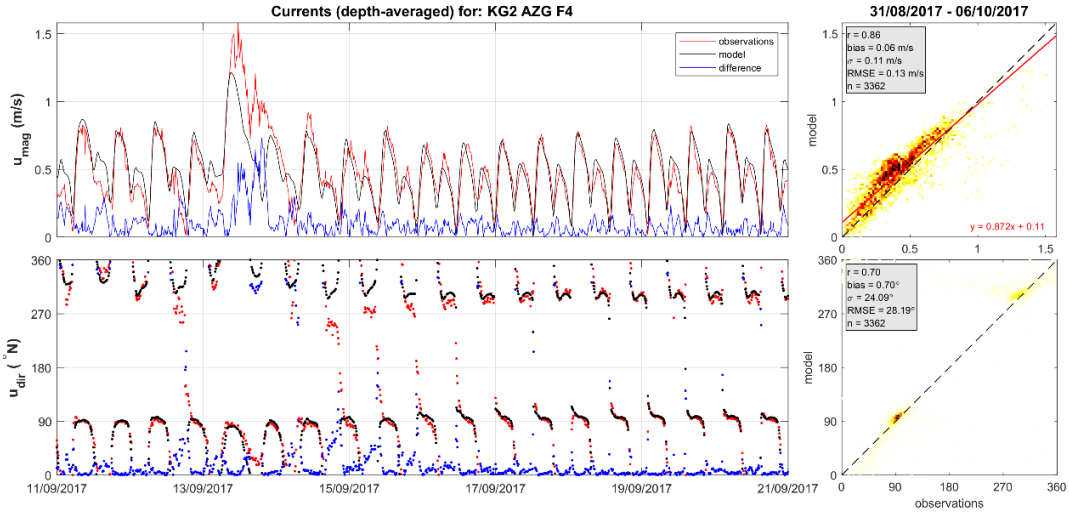

Figure 3.11 Timeseries of the magnitude (top) and direction (bottom) of depth-averaged flow velocities at observation point AZG F4 at the ebb-tidal delta in observations (in red) and in model results (in black).

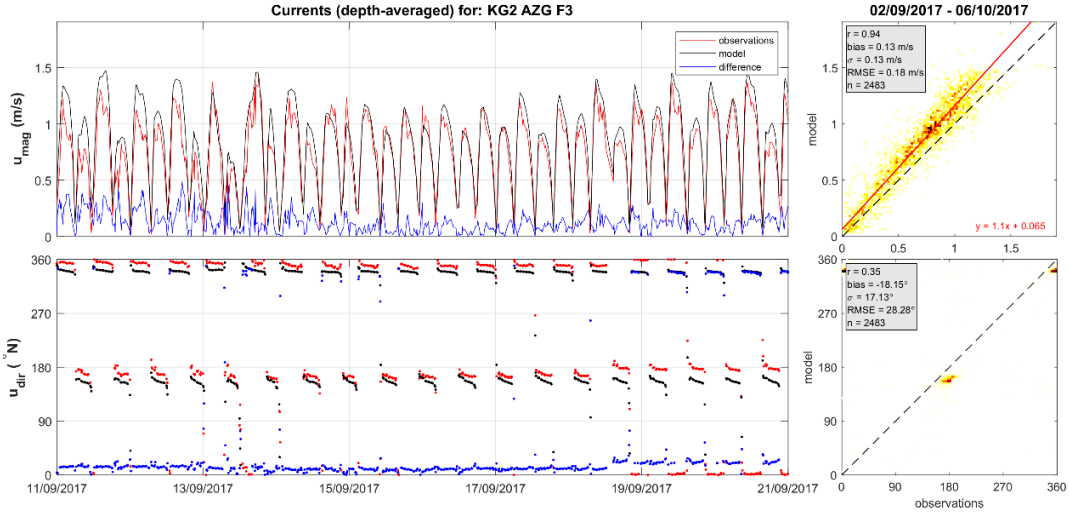

Figure 3.12 Timeseries of the magnitude (top) and direction (bottom) of depth-averaged flow velocities at observation point AZG F3 in the main channel in observations (in red) and in model results (in black).

The relatively large flow velocities at the observation point in the main channel of the tidal inlet are reproduced well by the model (r = 0.94, RMSE = 0.18 m/s; Figure 3.12). There is however a difference between the principal direction of the current in observations and the model results, which is reflected in a poor reproduction of the flow velocities in east-west direction (r = 0.52; Table 3.4). As the modelled flow velocities are aligned with the orientation of the main channel, there may be an error in the data that is available at AZG-F3.

Table 3.4 Linear correlation coefficient (r) and root-mean-square error (RMSE) of the reproduction of measured depth-averaged flow velocities at observation points around Ameland Inlet.

Station	**velocity magnitude**		**u (west-east)**		**v (south-north)**	
DVA lower shoreface	**r**	**RMSE [cm/s]**	**r**	**RMSE [cm/s]**	**r**	**RMSE [cm/s]**
DVA F1	0.95	7.3	0.99	8.3	-0.18	17.5
DVA F3	0.90	10.6	0.97	12.7	0.44	14.6
DVA F4	0.88	11.9	0.94	18.0	0.65	19.9
AZG ebb-tidal delta	**r**	**RMSE [cm/s]**	**r**	**RMSE [cm/s]**	**r**	**RMSE [cm/s]**
AZG F1	0.93	8.8	0.97	12.1	0.78	16.8
AZG F3	0.94	18.2	0.52	29.6	0.99	14.9
AZG F4	0.86	12.6	0.96	13.1	0.74	11.6
AZG F5	0.88	10.5	0.97	11.5	0.22	13.4

Figure 3.13 shows timeseries at observation point AqdA1 at the tidal divide of Ameland. These flow velocities at the tidal divides are very sensitive to the local bathymetry and water level variations. In general, the phasing of tidal flow variations is reproduced well by the model. Peak flow velocities after low water seem to be underestimated by the model, which may be caused by an overestimation of low water levels. Similar results are observed at the other observation points at the tidal divides of Terschelling and Ameland, as listed in Table 3.5. During the storm at September 13th, large eastward flows were observed at the tidal divides (Van Weerdenburg et al., 2021). This eastward flow is captured reasonably well in the model results, although the magnitude of the flow velocities is underestimated. The underestimation of the peak flow velocity appears to be more severe than the underestimation of the skew surge during this storm (-12% at Harlingen).

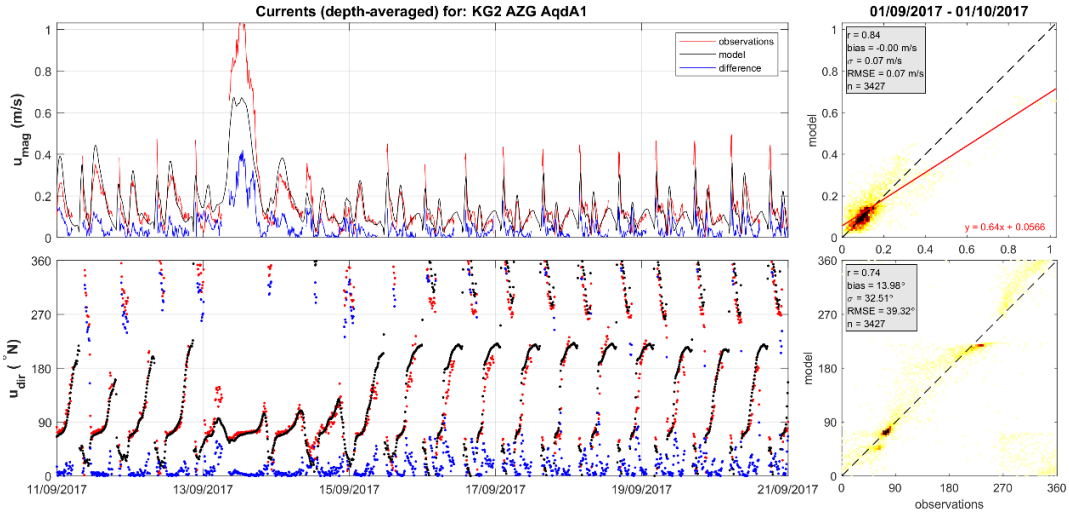

Figure 3.13 Timeseries of the magnitude (top) and direction (bottom) of depth-averaged flow velocities at observation point AZG AqdA1 at the tidal divide of Ameland in observations (in red) and in model results (in black).

Table 3.5 Linear correlation coefficient (r) and root-mean-square error (RMSE) of the reproduction of measured depth-averaged flow velocities at the tidal divides of Terschelling and Ameland.

Station	**velocity magnitude**	
AZG tidal divides	**r**	**RMSE [cm/s]**
AqdT1	0.78	13.0
AqdT2	0.79	13.4
AqdT3	0.85	7.8
AqdA1	0.84	6.7
AqdA2	0.86	8.4
AqdA3	0.86	12.1

Appendix A includes a comparison between the reproduction of measured flow velocities by DWSM and by another D-HYDRO model of the Dutch Wadden Sea, which is the WadSEA-FM Ameland model (Van Weerdenburg et al., 2021). In contrast to DWSM, the WadSEA-FM model is a two-dimensional, depth-averaged model. Multiple refinement steps provide a relatively high network resolution of around 30-50 m in Ameland Basin. Despite the difference in resolution with DWSM, the accuracy by which measured flow velocities are reproduced is on average similar for both models. Spatial differences in which of the two models is performing slightly better may be due to differences in bathymetry, partly caused by a large difference in resolution. Like in DWSM, the cross-shore currents at the lower foreshore are poorly reproduced by WadSEA-FM.

3.3 Discharges

DWSM results of discharges through Ameland Inlet are validated against measurements during three periods of 13 hours in September 2017. During these measurements, the discharge was measured along two transects by two vessels that were equipped with a downward-looking ADCP instrument (Van der Werf et al., 2019). The comparison is illustrated in Figure 3.15.

It follows from Figure 3.14 that the phasing and temporal variation of discharges through Ameland Inlet are well represented by DWSM. The computed discharges are slightly larger than measured discharges. The difference is about 7-10% of the integrated volume of water, which is considered to be within the same order of magnitude as the accuracy of the measurements. The computed discharges are a few percent larger than in the WadSEA-FM Ameland model (Van Weerdenburg et al., 2021); WadSEA-FM is overestimating the measured discharges less than DWSM (i.e., 2-6% instead of 7-10%). The differences in results from both models are likely caused by a higher model resolution in WadSEA-FM, the inclusion of (three-dimensional) baroclinic processes in DWSM as well as a difference in lateral boundary forcing.

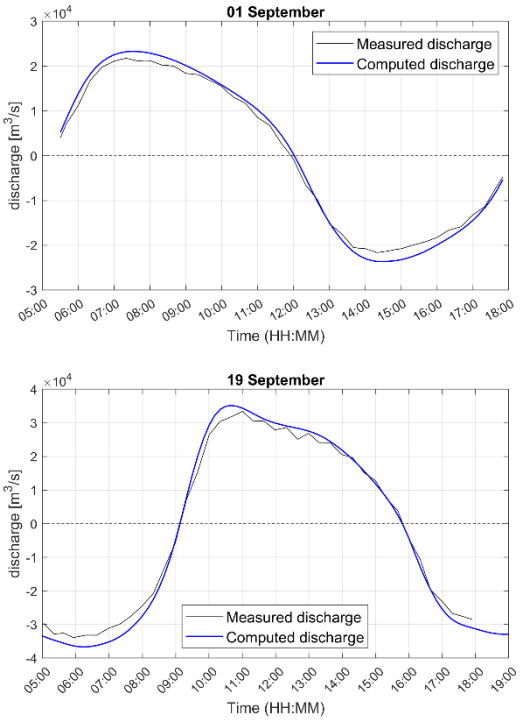

		Measured	Computed
01/09	**Qflood**	350*10^6 m^3	383*10^6 m^3 (+9%)
	Qebb	331*10^6 m^3	357*10^6 m^3 (+8%)
05/09	**Qflood**	467*10^6 m^3	514*10^6 m^3 (+10%)
	Qebb	462*10^6 m^3	507*10^6 m^3 (+10%)
19/09	**Qflood**	525*10^6 m^3	562*10^6 m^3 (+7%)
	Qebb	532*10^6 m^3	583*10^6 m^3 (+10%)

Figure 3.14 Comparison between measured and computed (DWSM) discharges through Ameland Inlet for three 13-hour periods in September 2017. The table lists integrated volumes in flood (negative) and ebb (positive) direction.

3.4 Residual discharges

The residual flows through the tidal inlets of the Wadden Sea are important for the large scale exchange flows between tidal basins in the Wadden Sea and the North Sea. Timeseries of DWSM model results of the residual discharges through the five tidal inlets in the Dutch Wadden Sea are shown in Figure 3.15. These timeseries show a residual inflow through the Vlie and Eierlandse Gat inlets, and a residual outflow through the Marsdiep, Borndiep and Friesche Zeegat inlets. The variations over time illustrate both seasonal variations as well as effects of short events (i.e., storms). The difference between the total outflow and the total residual inflow through these five inlets is caused by freshwater discharges, the difference between evaporation and precipitation, as well as the residual flow over the tidal divide of Schiermonnikoog. The residual discharges over the tidal divides of Terschelling, Ameland and Schiermonnikoog are shown in Figure 3.16, from which it follows that the residual discharge over the tidal divides becomes smaller towards the east in the Dutch Wadden Sea. This is mostly due to the decreasing conveyance area of tidal divides towards the east (i.e., the length of the tidal divide and the local water depth).

The residual discharges through the tidal inlets in the Western Dutch Wadden Sea have earlier been determined in a modelling study by Duran-Matute et al. (2016). As the residual discharge is largely determined by the meteorological forcing, it is difficult to compare the model results for different years. Nonetheless, the direction and temporal variations of the residual flow through the inlets in DWSM correspond with the results of Duran-Matute et al. (2016). The residual discharges in model results for 2017 are relatively large compared to the residual discharges in 2009-2011, which is caused by frequently occurring westerly winds in 2017. The residual discharges through Ameland Inlet and over the tidal divides of Terschelling and Ameland are very similar to those found in Van Weerdenburg et al. (2021). Small differences may follow from a difference in network resolution and by the inclusion of (three-dimensional) baroclinic processes in DWSM.

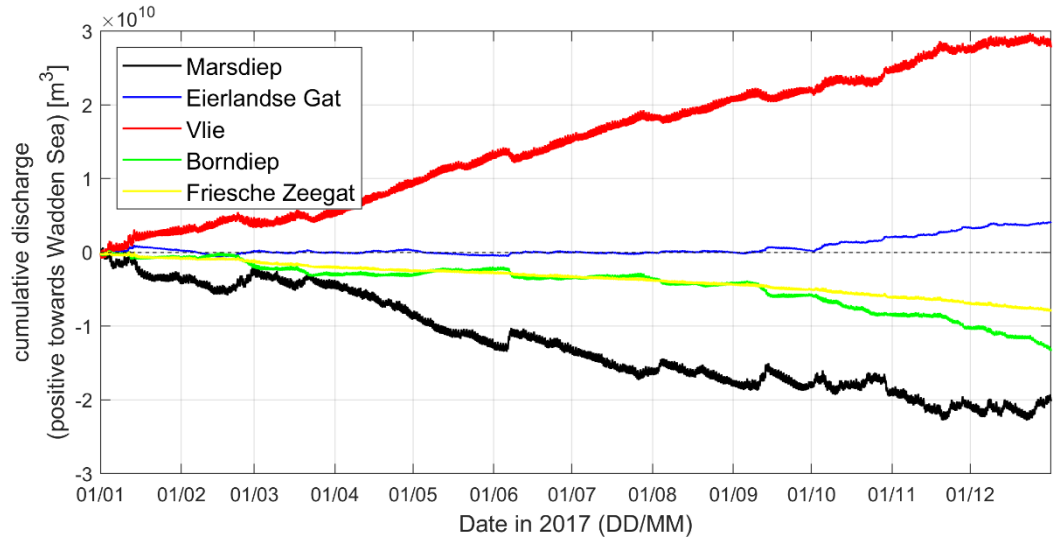

Figure 3.15 Timeseries of the cumulative discharges through tidal inlets in the Dutch Wadden Sea from a DWSM model simulation for 2017.

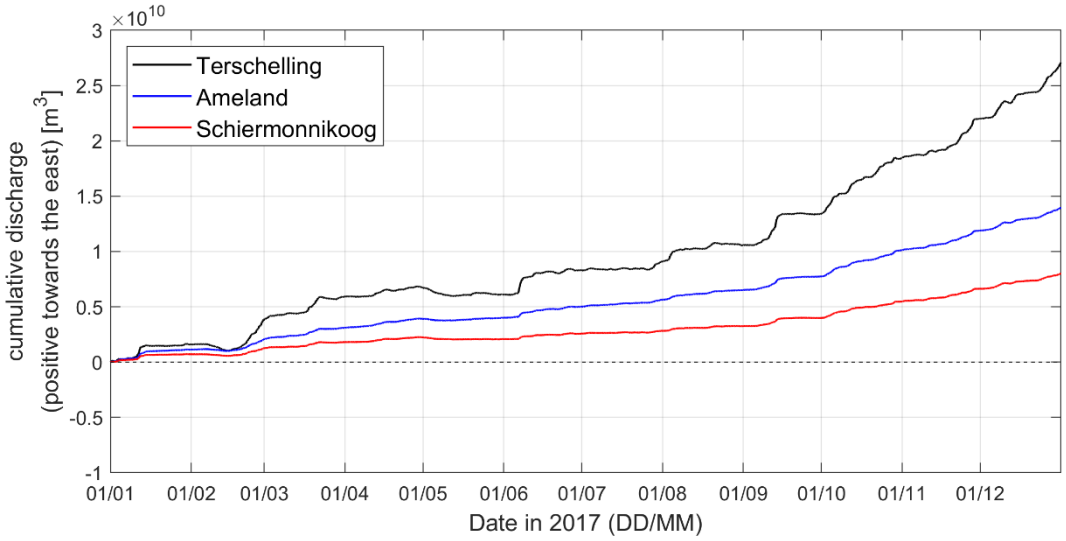

Figure 3.16 Timeseries of the cumulative discharges over the tidal divides of Terschelling, Ameland and Schiermonnikoog from a DWSM model simulation for 2017.

3.5 Salinity

In this section, the computed sea surface salinity is compared to in-situ measurements. This is first done for the North Sea part of the domain, where model results are compared to MWTL measurements in the parts of the Terschelling and Rottumerplaat transects that are covered by the DWSM domain. The statistics are presented in Table 3.6, which includes 3D DCSM-FM and the first release of DWSM for comparison. As an example, a time series and scatter plot for station Terschelling 10 km is shown in Figure 3.17. In general, the sea surface salinity is well represented in DWSM, with a comparable quality to 3D DCSM-FM. The exception is station Rottumerplaat 3 km, where the RMSE is 0.94 psu in DWSM, which is an improvement upon the 1.52 psu in 3D DCSM-FM. Compared to the first release of DWSM, the quality of salinity representation (in terms of RMSE) in the North Sea part of the domain has improved in most stations.

Table 3.6 Comparison of the quality of the sea surface salinity representation in DWSM (first and second release) and 3D DCSM-FM at the Terschelling and Rottumerplaat transect, in terms of bias, standard deviation (std) and Root-Mean-Square Error (RMSE).

Station	Bias (psu)			Std (psu)			RMSE (psu)		
	3D DCSM-FM	DWSM 1st rel.	DWSM 2nd rel.	3D DCSM-FM	DWSM 1st rel.	DWSM 2nd rel.	3D DCSM-FM	DWSM 1st rel.	DWSM 2nd rel.
Terschelling 10 km	0.07	-0.25	0.08	0.45	0.59	0.42	0.46	0.64	0.42
Terschelling 50 km	-0.02	-0.10	-0.04	0.29	0.27	0.33	0.29	0.29	0.34
Rottumerplaat 3 km	-1.33	-0.97	-0.60	0.73	0.80	0.73	1.52	1.25	0.94
Rottumerplaat 50 km	0.15	0.05	0.13	0.35	0.46	0.35	0.38	0.46	0.37

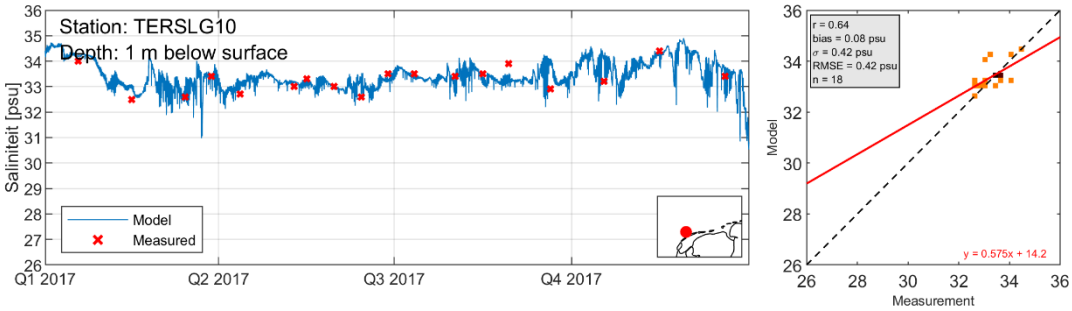

Figure 3.17 Time series and scatter plot of computed (DWSM; second release) and measured sea surface salinity for station Terschelling 10 km.

A similar comparison is made for stations in the Wadden Sea in Table 3.7. In addition, the DWSM results for Dantziggat are plotted in Figure 2.1. Errors in terms of RMSE are larger than in the North Sea, but this can be explained by the larger temporal and spatial variability. Compared to 3D DCSM-FM the quality has improved in all four stations (in terms of RMSE), while compared to the first release of DWSM three out of four stations improve. The improvement is especially large for station Dantziggat, where the RMSE almost halves (from 2.22 psu to 1.16 psu).

Table 3.7 Comparison of the quality of the sea surface salinity representation in DWSM (first and second release) and 3D DCSM-FM at station in the Wadden Sea, in terms of bias, standard deviation (std) and Root-Mean-Square Error RMSE.

Station	Bias (psu)			Std (psu)			RMSE (psu)		
	3D DCSM-FM	DWSM 1st rel.	DWSM 2nd rel.	3D DCSM-FM	DWSM 1st rel.	DWSM 2nd rel.	3D DCSM-FM	DWSM 1st rel.	DWSM 2nd rel.
DANTZGT	-1.38	-1.64	-0.29	1.50	1.50	1.12	2.04	2.22	1.16
DOOVBWT	0.10	-0.83	-0.44	1.97	1.60	1.58	1.97	1.80	1.64
MARSDND	0.27	-0.83	-0.39	1.72	1.55	1.36	1.75	1.76	1.42
VLIESM	0.36	0.09	0.32	0.92	0.90	0.86	0.99	0.90	0.92

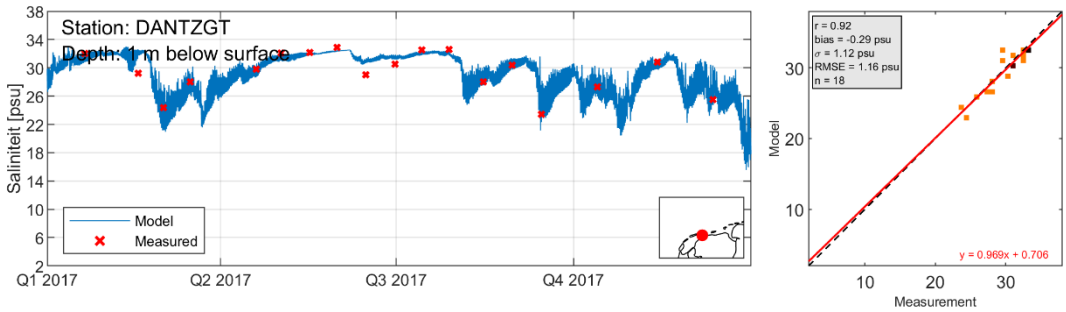

Figure 3.18 Time series and scatter plot of computed (DWSM) and measured sea surface salinity for station Dantziggat.

At the NIOZ Jetty measurements are available with a high temporal resolution. The computed timeseries of the salinity at the NIOZ jetty (Figure 3.19) show a good representation of these observed values. Statistics on the accuracy are listed in Table 3.8 and are slightly better than 3D DCSM-FM in terms of RMSE, despite a larger bias. Compared to the first release of DWSM, the bias reduces substantially (from -0.74 psu to -0.19 psu), while the RMSE has also improved (from 1.46 psu to 1.22 psu).

Table 3.8 Comparison of the quality of the sea surface salinity representation in DWSM (first and second release) and 3D DCSM-FM at station NIOZ Jetty, in terms of bias, standard deviation (std) and Root-Mean-Square Error RMSE.

Station	Bias (psu)			Std (psu)			RMSE (psu)		
	3D DCSM-FM	DWSM 1st rel.	DWSM 2nd rel.	3D DCSM-FM	DWSM 1st rel.	DWSM 2nd rel.	3D DCSM-FM	DWSM 1st rel.	DWSM 2nd rel.
NIOZ Jetty	0.10	-0.74	-0.19	1.38	1.26	1.21	1.38	1.46	1.22

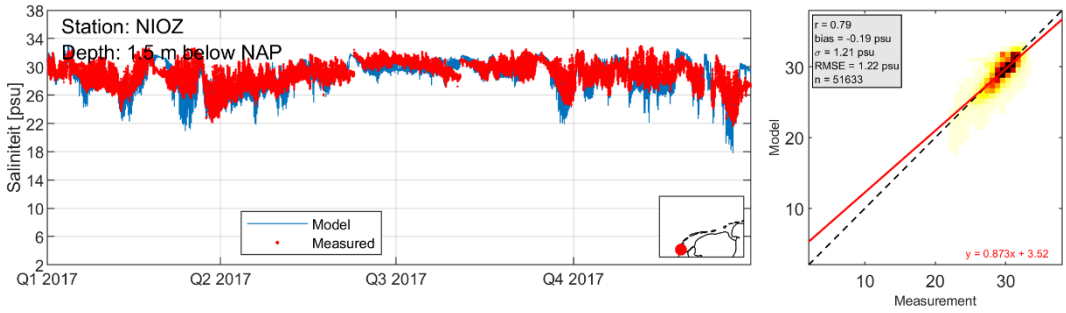

Figure 3.19 Time series and scatter plot of computed (DWSM) and measured sea surface salinity for station NIOZ Jetty.

3.6 Temperature

In this section, the computed sea surface temperature is compared to in-situ measurements. This is first done for the North Sea part of the domain, where model results are compared to MWTL measurements in the parts of the Terschelling and Rottumerplaat transects that are covered by the DWSM domain. The statistics are presented in Table 3.9, which includes 3D DCSM-FM for comparison. As an example, a time series and scatter plot for station Terschelling 10 km is shown in Figure 3.20. The sea surface temperature is well represented in DWSM, with a quality that is comparable to 3D DCSM-FM. The exception is Rottumerplaat 3 km, which significantly improves. The RMSE values are around 0.3-0.4 °C, while the bias is slightly negative in all four stations, ranging from -0.1 °C to -0.5 °C.
Compared to the first release of DWSM, the improvement in quality is striking. The bias reduces from 0.9-1.3 °C in the first release, to 0.1-0.4 °C in the present release. This also contributes to a large reduction in RMSE, by a factor 3-4 (from 1.0-1.6 °C to 0.3-0.4 °C).

Table 3.9 Comparison of the quality of the sea surface temperature representation in DWSM (first and second release) and 3D DCSM-FM at the Terschelling and Rottumerplaat transect, in terms of bias, standard deviation (std) and Root-Mean-Square Error (RMSE).

Station	Bias (°C)			Std (°C)			RMSE (°C)		
	3D DCSM-FM	DWSM 1st rel.	DWSM 2nd rel.	3D DCSM-FM	DWSM 1st rel.	DWSM 2nd rel.	3D DCSM-FM	DWSM 1st rel.	DWSM 2nd rel.
Terschelling 10 km	-0.22	-0.94	-0.26	0.23	0.42	0.20	0.32	1.03	0.33
Terschelling 50 km	-0.09	-0.95	-0.11	0.35	0.46	0.40	0.36	1.06	0.41
Rottumerplaat 3 km	-0.51	-1.23	-0.36	0.35	0.96	0.24	0.62	1.56	0.43
Rottumerplaat 50 km	-0.28	-1.33	-0.30	0.08	0.33	0.13	0.29	1.37	0.33

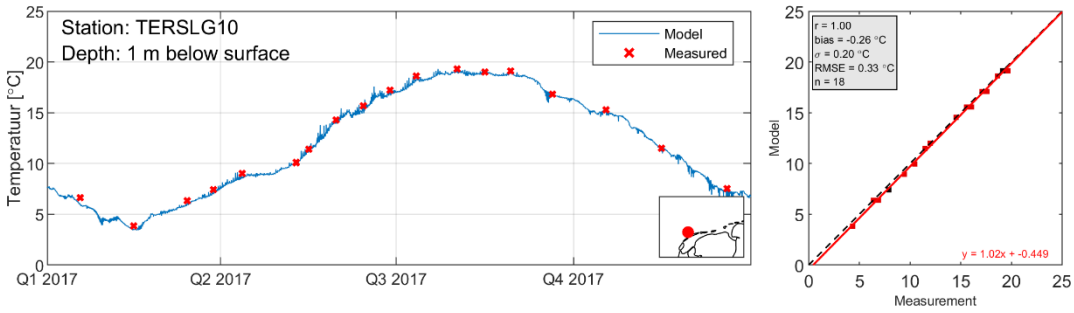

Figure 3.20 Time series and scatter plot of computed (DWSM) and measured sea surface temperature for station Terschelling 10 km.

A similar comparison is made for stations in the Wadden Sea in Table 3.10. In addition, the DWSM results for Marsdiep Noord (MARSDND) are plotted in Figure 3.21. Errors in terms of RMSE are between 0.3 °C and 0.6 °C, which is slightly larger than in the North Sea, but still very good given the coarse resolution of the meteorological forcing. The DWSM quality with respect to sea surface temperature is similar to 3D DCSM-FM, while the improvement compared to the first release of DCSM is substantial. Both a reduction in bias and standard deviation contribute to a reduction in RMSE with a factor of approximately four.

Table 3.10 Comparison of the quality of the sea surface temperature representation in DWSM (first and second release) and 3D DCSM-FM at station in the Wadden Sea, in terms of bias, standard deviation (std) and Root-Mean-Square Error RMSE.

Station	Bias (°C)			Std (°C)			RMSE (°C)		
	3D DCSM-FM	DWSM 1st rel.	DWSM 2nd rel.	3D DCSM-FM	DWSM 1st rel.	DWSM 2nd rel.	3D DCSM-FM	DWSM 1st rel.	DWSM 2nd rel.
DANTZGT	-0.55	-2.30	-0.44	0.44	1.31	0.46	0.70	2.65	0.64
DOOVBWT	-0.37	-1.89	-0.42	0.32	0.98	0.24	0.49	2.12	0.48
MARSDND	-0.24	-1.30	-0.29	0.27	0.72	0.20	0.35	1.48	0.36
VLIESM	-0.25	-1.07	-0.27	0.24	0.71	0.22	0.35	1.28	0.35

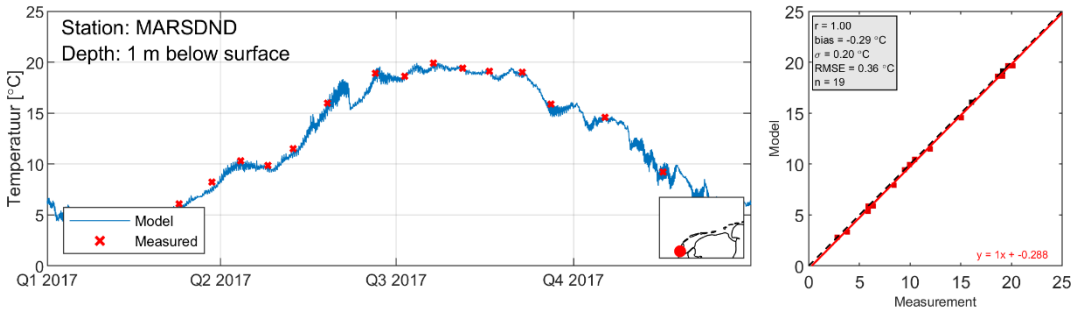

Figure 3.21 Time series and scatter plot of computed (DWSM) and measured sea surface temperature for station Marsdiep Noord.

At the NIOZ Jetty measurements are available with a high temporal resolution. The computed timeseries of the sea surface temperature at the NIOZ jetty (Figure 3.22) show a good representation of these observed values. Statistics on the accuracy are listed in Table 3.11 and show a similar quality as 3D DCSM-FM. Compared to the first release of DWSM, the model quality has improved substantially. The bias, standard deviation and RMSE have all reduced by a factor of 3-4.

Table 3.11 Comparison of the quality of the sea surface temperature representation in DWSM (first and second release) and 3D DCSM-FM at station NIOZ Jetty, in terms of bias, standard deviation (std) and Root-Mean-Square Error RMSE.

Station	Bias (°C)			Std (°C)			RMSE (°C)		
	3D DCSM-FM	DWSM 1st rel.	DWSM 2nd rel.	3D DCSM-FM	DWSM 1st rel.	DWSM 2nd rel.	3D DCSM-FM	DWSM 1st rel.	DWSM 2nd rel.
NIOZ Jetty	-0.23	-1.25	-0.29	0.42	0.85	0.37	0.48	1.51	0.47

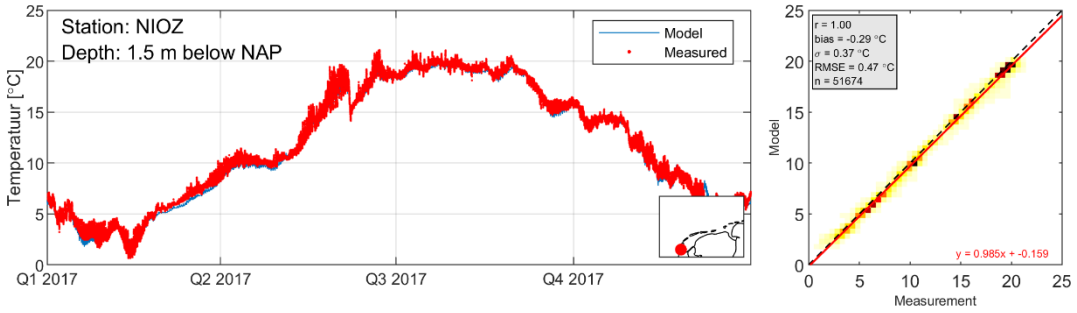

Figure 3.22 Time series and scatter plot of computed (DWSM) and measured sea surface temperature for station NIOZ Jetty.

4 Validation – Mud dynamics

4.1 Introduction

Model validation on mud dynamics was carried out in the same way as reported by Vroom et al. (2020). The validation focuses on suspended sediment concentration averages, their spatial gradients and temporal variations, bed composition and residual transport. These are discussed in the following sections.

4.2 Time-averaged sediment concentrations

Time-averaged sediment concentrations are validated against MWTL measurements of the suspended particulate matter (SPM) near the water surface at observations points. Twelve observations points in the DWSM model domain were part of the MWTL measurement program in 2017 (i.e. the year for which the model is validated). Table 4.1 lists the number of measurements (N) and the average SPM (μ) for each of the observation points in 2017, but also for the longer period of MWTL measurements from 1989[1] until 2017. Table 4.1 also lists time-averaged DWSM-Mud model results for the first release of the model (Vroom et al., 2020) and for the second release of the model (described in this report). The time-averaged model results are based on timeseries with a time interval of Δt = 10 min. The SPM measurements and modelled timeseries are illustrated in Figure 4.1.

As the number of MWTL observation points that were measured in 2017 is limited, the model results are also validated against MWTL measurements from before 2017 at different observation points. These results are included in Figure 4.2. In contrast to the results in Table 4.1, measurement data from before 1989 has been used in these results, such that as many observations points as possible are included in the validation.

From the MWTL measurements it follows that the average SPM in 2017 may deviate significantly from the long-term average SPM. For example, at observation point VLIESM, the SPM is almost two times as high in 2017 than averaged over 1989-2017. This may both be induced by actual fluctuations in the average SPM between years, but also by the limited number of measurements per year (i.e. such that the average over the measured values does not necessarily represent the average SPM in a year).

At most observation points, the reproduction of SPM measurements by DWSM-Mud is reasonably good. The average SPM at deep observation points in the Wadden Sea and along the North Sea coast of the Wadden Islands (DOOVBWT, MARSDND, VLIESM and BOOMKDP) is similar in measurements and in model results. The average SPM at DANTZGT is slightly underestimated by the model.

Relatively large mean SPM at Holwerd (HOLWD) and in the Ems-Dollard estuary (BOCHTVWTM and GROOTGND) are underestimated by the model. This may be due to the limited horizontal and vertical resolution of the model. In addition, certain processes such as flocculation and the effect of high sediment concentrations on the fluid density may be important at these locations but are not reproduced in the model.

[1] Data from before 1989 has not been used to compute the average SPM that is listed in Table 4.1, because the MWTL measurement procedure has only been consistent since 1989.

In general, model results of the new (2nd) release of DWSM-Mud are similar to the results of the first release (Vroom et al., 2020). Differences are expected to originate from changes in the bathymetry and the model formulations for wave stirring, which are both very important for the amount of resuspension from the seabed.

Table 4.1 Number of MWTL measurements (N) and average SPM (μ) at observations points and time-averaged sediment concentrations in DWSM-Mud results (1st and 2nd release of the model).

Station	MWTL data 2017		MWTL data 1989-2017		DWSM-Mud results 2017	
					DWSM 1st rel.	DWSM 2nd rel.
	N	μ (mg/L)	N	μ (mg/L)	μ (mg/L)	μ (mg/L)
BOCHTVWTM	18	106.7	471	116.6	9.9	18.5
BOOMKDP	18	15.4	188	29.3	26.0	10.4
DANTZGT	18	84.8	671	97.7	64.7	48.0
DOOVBWT	19	16.5	517	22.7	17.9	17.5
GROOTGND	19	211.0	526	147.0	49.0	55.4
HUIBGOT	19	13.6	526	15.6	32.6	36.4
MARSDND	19	18.5	524	27.4	17.9	16.4
ROTTMPT3	12	28.2	225	25.0	48.0	61.4
ROTTMPT50	6	4.8	172	3.5	2.2	2.4
TERSLG10	18	8.0	434	5.1	4.6	4.2
TERSLG50	18	6.1	331	5.0	1.6	1.4
VLIESM	12	15.8	338	26.7	31.1	25.6

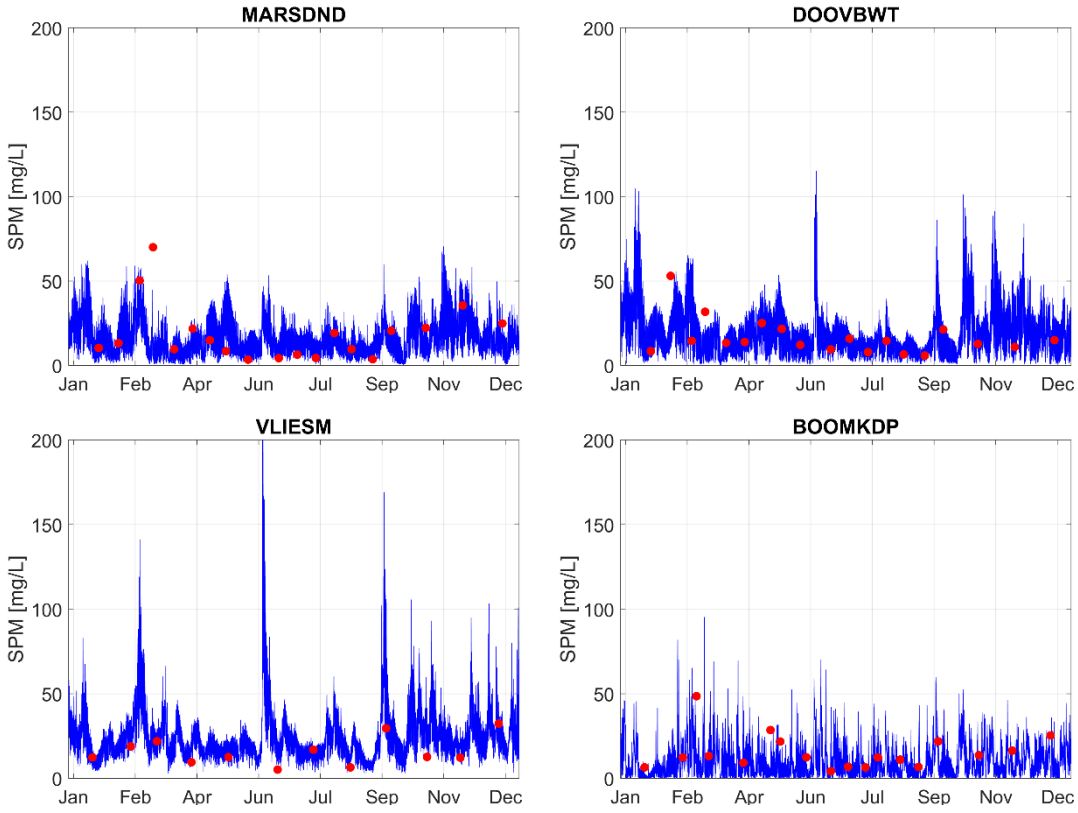

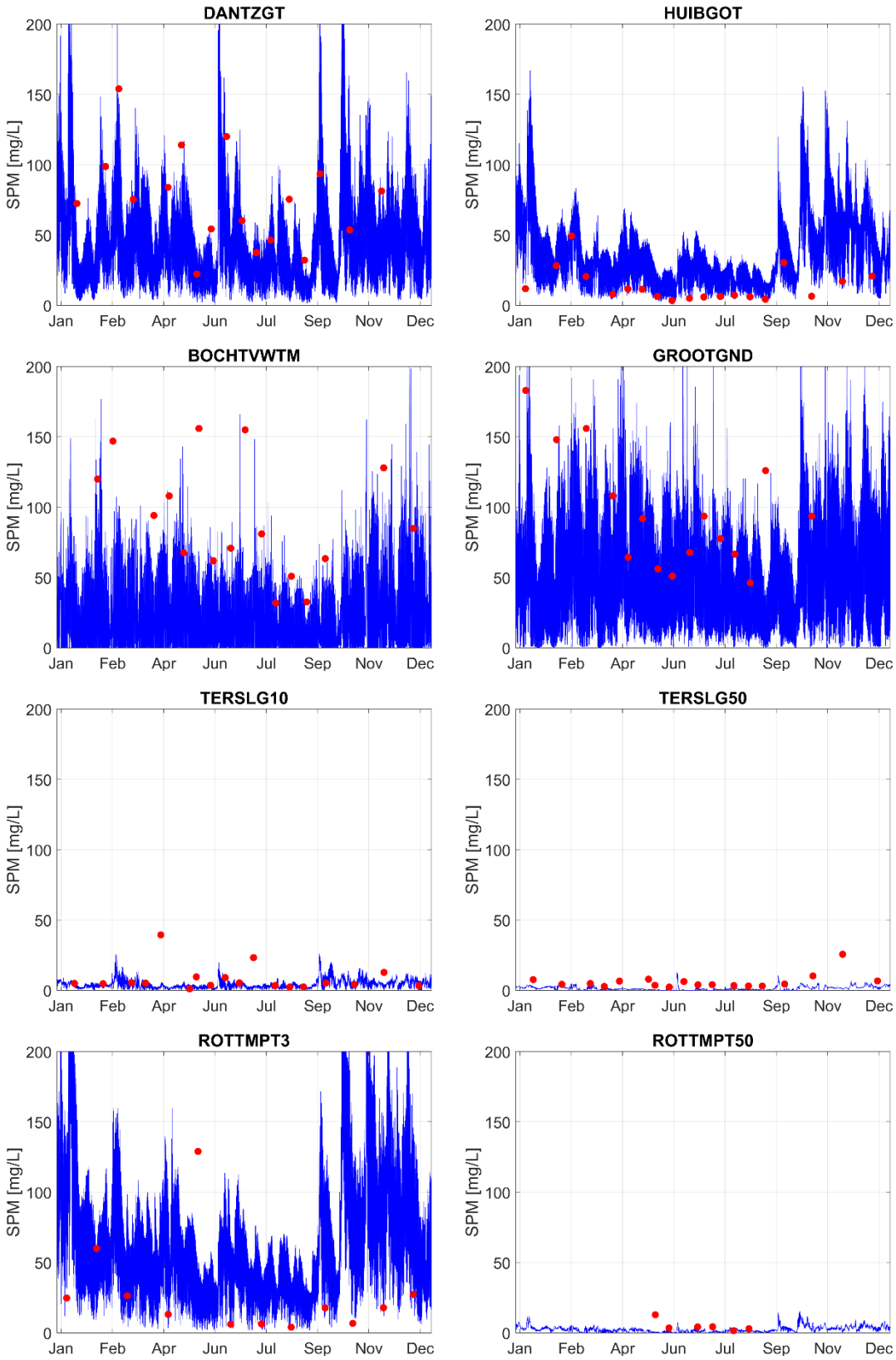

Figure 4.1 Timeseries of MWTL measurements (red dots) and DWSM-Mud model results (blue line) in 2017 at observation points in the Wadden Sea, Ems-Dollard estuary and the North Sea.

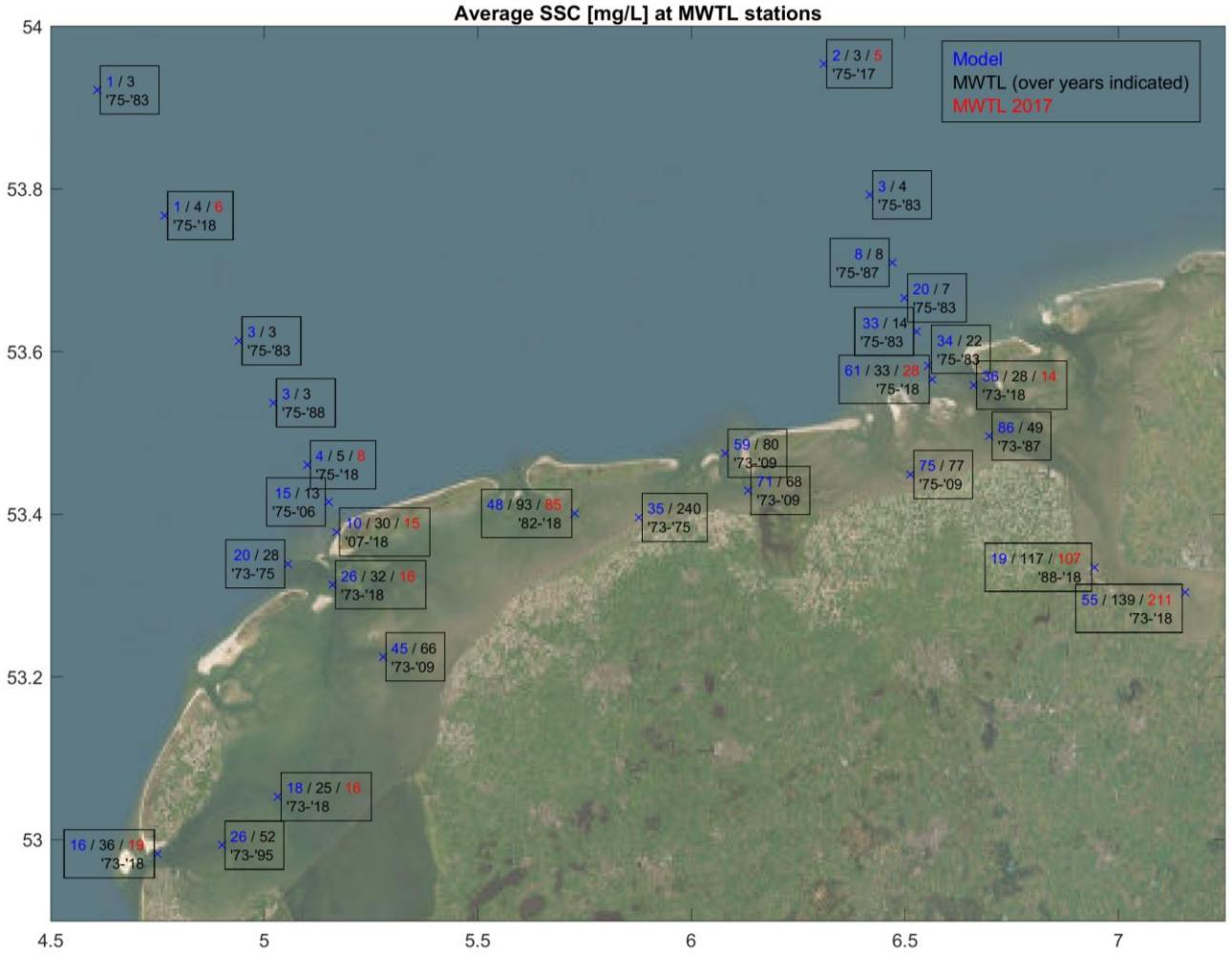

Figure 4.2 Comparison between measured and computed average SPM values near the water surface at MWTL observation points. DWSM-Mud results are listed in blue. The multi-year average SPM in observations are listed in black (i.e. average over measurements in the indicated period). The average SPM over measurements in 2017 are listed in red.

It becomes clear from the validation with MWTL measurements that the spatial variations in mean SPM are reasonably well reproduced by the model. These spatial variations in model results of the SPM are also illustrated in Figure 4.3 for 2017 and in Figure 4.4 for the months June and October.

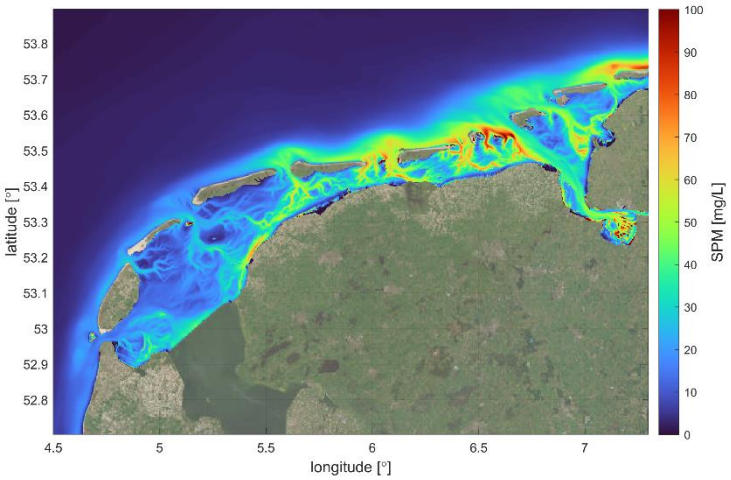

Figure 4.3 Model results for the average SPM near the water surface in 2017. Note that the computed SPM is zero for dry areas, such that the results at intertidal areas are biased by the exposure time.

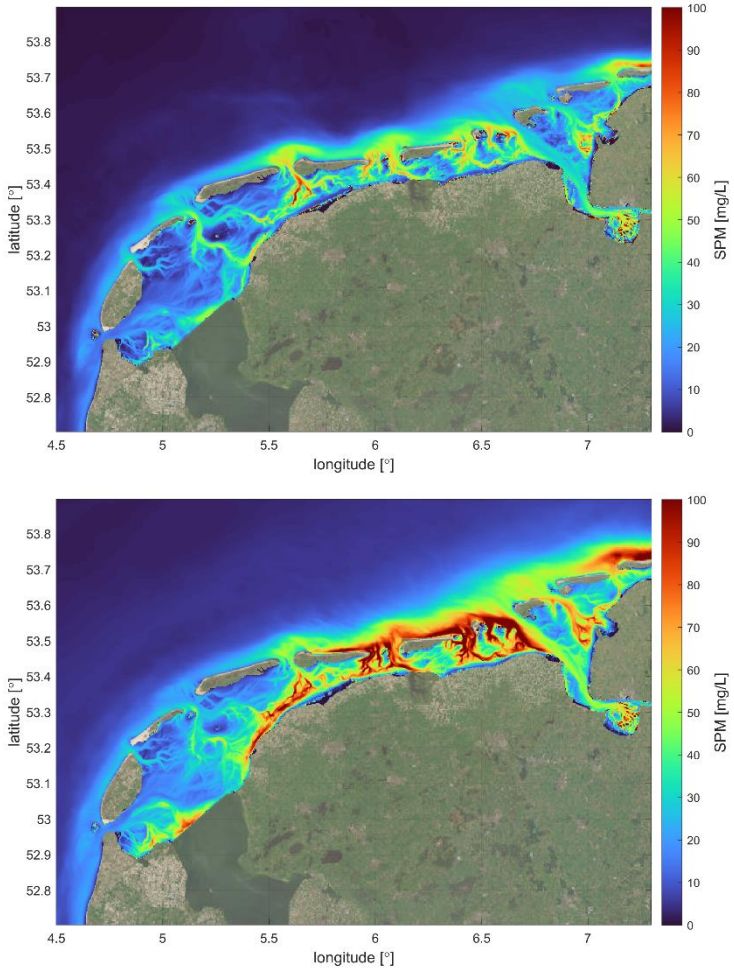

Figure 4.4 Model results for the average SPM near the water surface in June 2017 (top) and in October 2017 (bottom). Note that the computed SPM is zero for dry areas, such that the results at intertidal areas are biased by the exposure time.

4.3 Seasonal variations in sediment concentrations

Herman et al. (2018) found a strong seasonal variation in MWTL measurements of the SPM in the Wadden Sea and the North Sea. This seasonal variation is illustrated in Figure 4.5. To a large extent, this seasonal variation is reproduced in the model results for 2017, as is illustrated in Figure 4.6. Note that the observed variation in Figure 4.5 is based on multi-year averaged SPM measurements and the model results only cover 2017, such that the seasonal variation in the model results is largely affected by (stochastic) conditions in 2017. For example, the strong increase in SPM in Fall 2017 compared to multi-year averaged observations is due to the storm conditions in September 2017.

Note that biological processes may also cause a strong seasonal variation in SPM (e.g. Andersen et al., 2005; Pivato et al., 2019), but these processes are not included in the DWSM-Mud model.

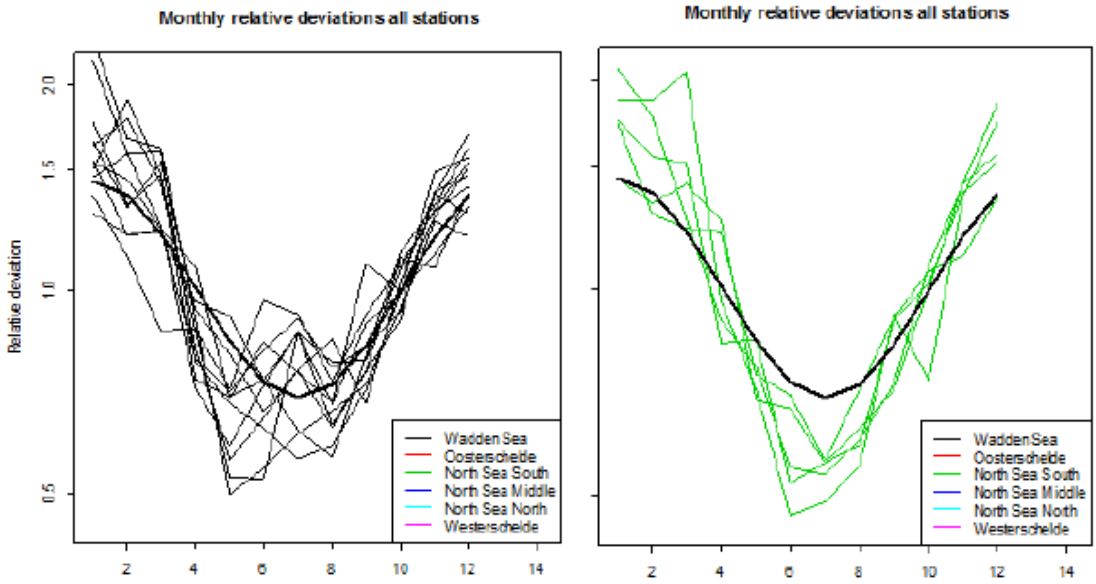

Figure 4.5 Mean relative deviation from the long-term average SPM per month in MWTL measurements from 1989-2017 in the Wadden Sea (left) and in the North Sea (right; Herman et al., 2018).

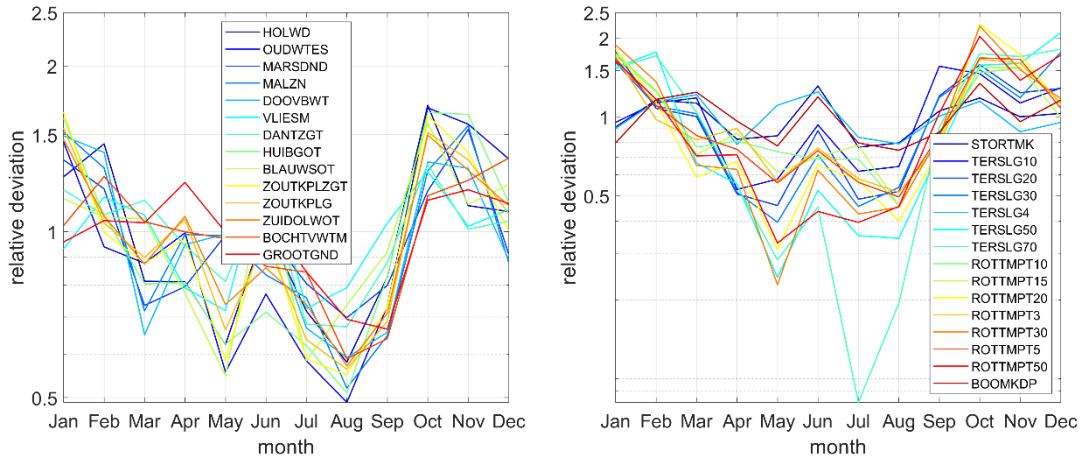

Figure 4.6 Mean relative deviation from the long-term average SPM per month in DWSM-Mud results for 2017 at MWTL observation points in the Wadden Sea (left) and in the North Sea (right).

4.4 Intra-tidal and vertical variations in sediment concentrations

The observed and computed suspended sediment concentrations near Eemshaven (Figure 4.7) and Boontjes (Figure 4.8) illustrate intra-tidal variations. Although there are no measurements available at Boontjes in 2017, the comparison of model results with data from 2012 indicates variations during tidal periods and during the spring-neap cycle that are not captured in MWTL measurements.

These results in Figure 4.7 and Figure 4.8 are very similar to the model results of the first release of the model (Vroom et al., 2020). The intra-tidal variation in the model results near Eemshaven is much smaller than in the observations. The phasing and tidal asymmetry (i.e. peaks in SPM are approximately equal during ebb and flood) are similar in observations and model results (bottom window in Figure 4.7), but the amplitude of intra-tidal fluctuations is underestimated by approximately a factor 2. This is probably the consequence of the reduced deposition efficiency in the model, such that the sediment concentrations remain relatively high during flow reversal. The reduced deposition efficiency is used to keep the average sediment concentrations in the model sufficiently high. The seasonal and spring-neap variations in the observations near Eemshaven is clearly reproduced in the model results (top and middle window in Figure 4.7).

The observed sediment concentrations near Boontjes are estimated by assuming a conversion factor of 1.7 from the turbidity (in NTU) to the suspended sediment concentration (in mg/L). In the observations, the peaks in SPM during ebb and flood are similar in height near the seabed (i.e. at -3 m NAP), but the peak during flood seems to be higher near the water surface (i.e. at -0.75 m NAP). In the model results, the asymmetry in the intra-tidal variations is present both near the seabed and near the water surface.

The measurements at Boontjes also reveal vertical variations in SPM. One important observation in comparison with the model results is that the SPM during flow reversal (i.e. just after high- and low water) is similar near the seabed and the water surface. In model results, however, the SPM near the seabed remains larger than near the water surface. This seems to be largely caused by the fact that the sediment concentrations in the model remain relatively high during flow reversal, as was already addressed earlier in this section.

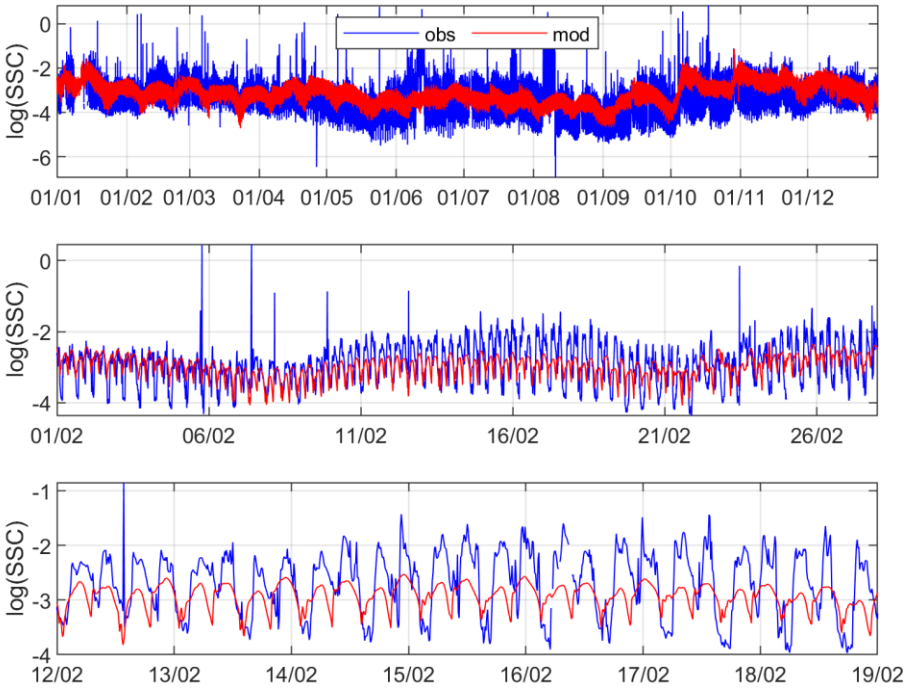

Figure 4.7 Observed (red) and computed (blue) sediment concentrations near Eemshaven in 2017. The three windows show the same results at different time intervals. Note that the suspended sediment concentrations on the vertical axis are log-transformed.

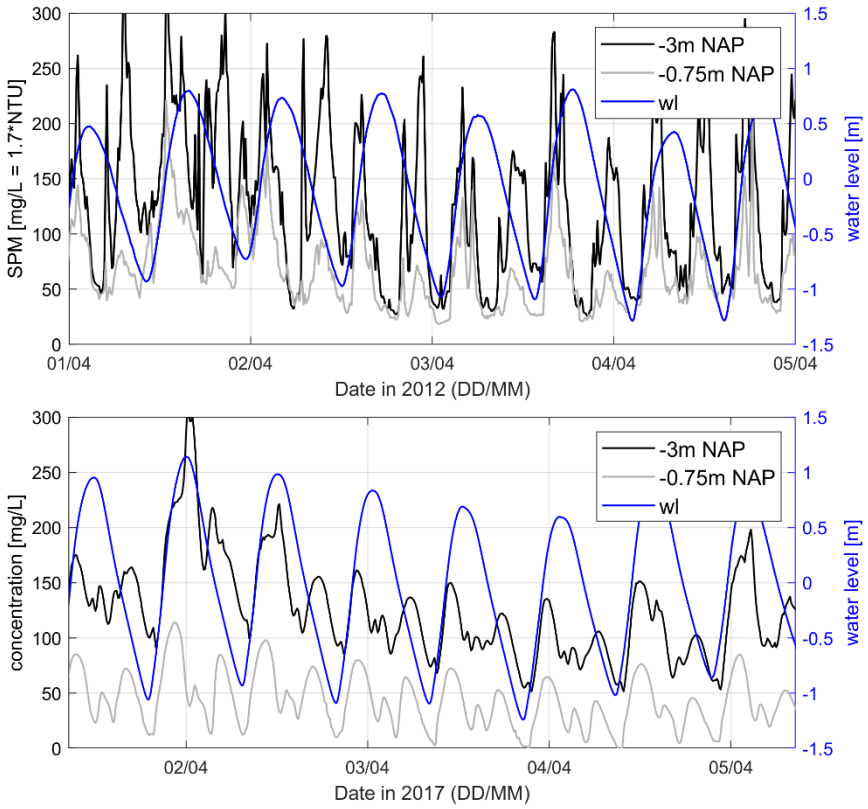

Figure 4.8 Sediment concentrations near Boontjes in observations in 2012 (top) and in model results for 2017 (bottom). Black and grey lines indicate sediment concentrations at -3 m NAP -0.75 m NAP, respectively.

4.5 Bed sediment composition

As discussed in Section 2.11, the initial condition of mud in the bed is the result of a series of spin-up simulations with a total duration of three years, after using the measured mud fraction in the seabed (Sediment Atlas of the Wadden Sea) as the initial conditions for the first simulation. The amount of mud in the seabed at the end of the three-year spin-up period and thus the initial condition for model simulations of 2017 is illustrated in Figure 4.9. The amount of mud in the seabed is particularly high along the mainland coast, at the tidal divides and in parts of the Ems-Dollard estuary. After a simulation of one year (see Figure 4.9), the net change in the amount of mud in the seabed is relatively small. This confirms that the spatial distribution of mud in the seabed is indeed close to a dynamic equilibrium.

The mud fraction with the larger settling velocity is much more present in the bed than the mud fraction with the smaller settling velocity, as is illustrated in Figure 4.10. This confirms that the 80:20 distribution between the two sediment fractions in the bed that was imposed at the start of the spin-up period (see 2.11.4) was a reasonable estimation.

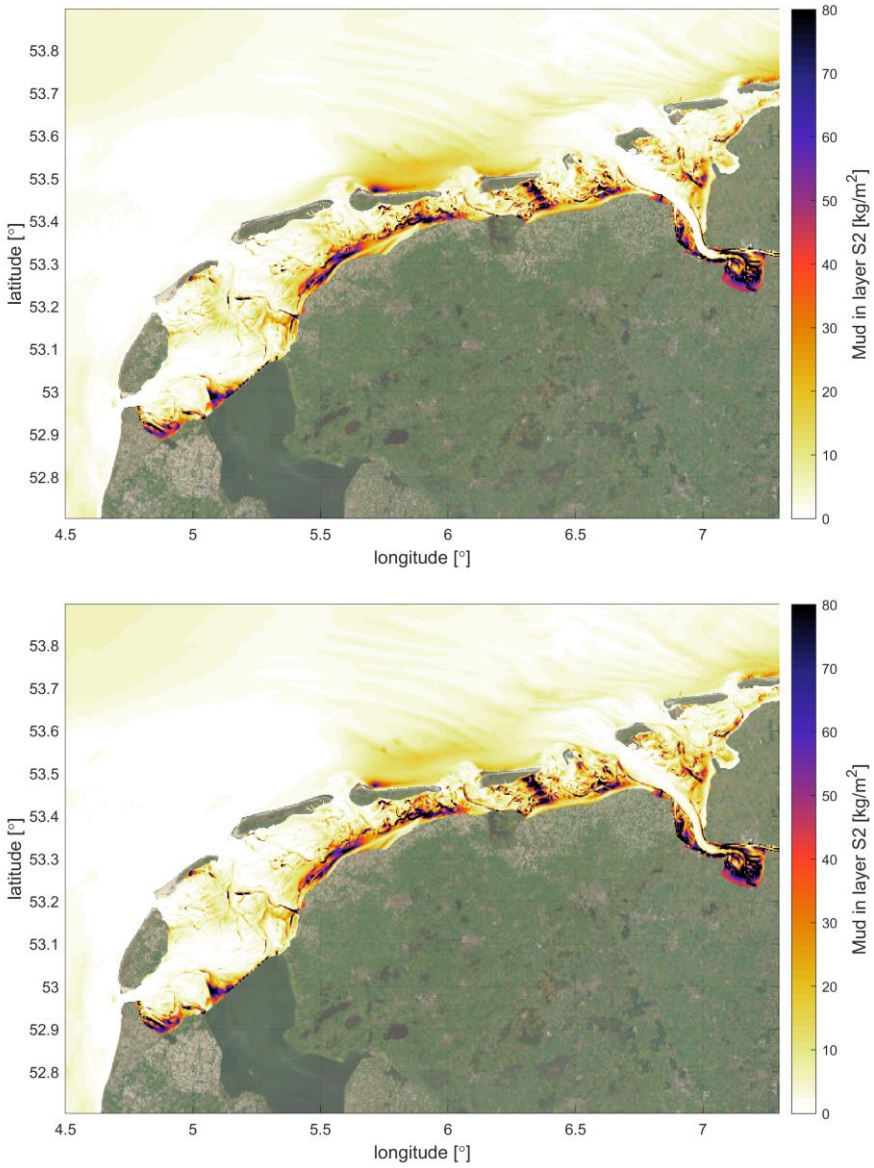

Figure 4.9 Amount of mud in the seabed (layer S2) at the start (i.e. on 01-01-2017; top) and at the end (i.e. on 01-01-2018; bottom) of a one year simulation period.

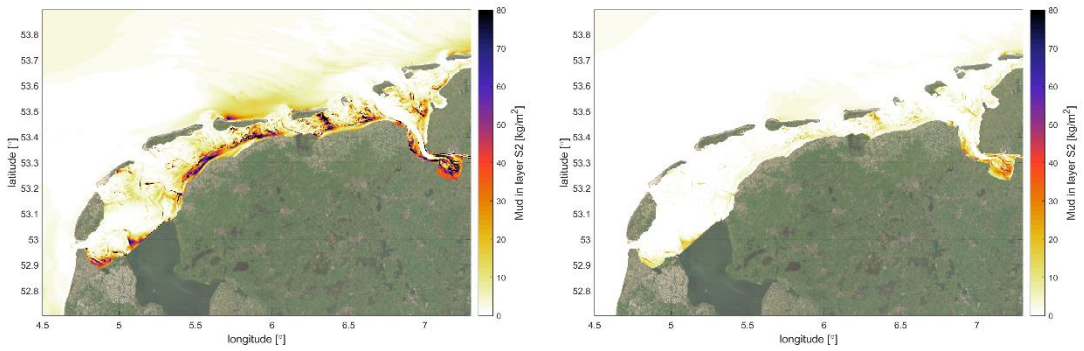

Figure 4.10 Amount of mud fraction IM1 (left) and IM2 (right) in the seabed (layer S2) after the spin-up period, hence at the start (i.e. on 01-01-2017) of model simulations.

4.6 Residual transport and the mud balance of the Wadden Sea

Model results of the residual mud transports through the tidal inlets and over the tidal divide of Schiermonnikoog together form a mud balance of the Dutch Wadden Sea. These transports are illustrated in Figure 4.8 and the cumulative results are listed in Table 4.2. In 2017, there is a residual import of mud through the three westernmost inlets (i.e. Marsdiep, Eierlandse Gat and Vlie). There is an export of mud from the Dutch Wadden Sea through the Borndiep and Friesche Zeegat and over the tidal divide of Schiermonnikoog. The sum of these residual import and export rates over 2017 is close to zero, such that the total amount of mud in the Wadden Sea at the end of the year is close to what it was at the beginning of the year. The model results of 2017 therefore do not reproduce the long-term averaged residual import of mud into the Wadden Sea that is observed in field data (Oost et al., 2021; Colina Alonso et al., 2021). It is however difficult to evaluate the model performance based on this outcome, as earlier studies have also shown that the observed wind conditions in 2017 were favorable for eastward residual transport (Vroom et al., 2020; Van Weerdenburg et al., 2021), hence limiting the sediment accumulation in the Wadden Sea.

The timeseries in Figure 4.8 show a clear seasonal variation, in which the amount of mud in the Wadden Sea is larger in summer than in winter, caused by a relatively large residual export of mud through the Borndiep and Friesche Zeegat and over the tidal divide of Schiermonnikoog in autumn and winter.

The residual transport rates over the tidal divides of Terschelling, Ameland and Schiermonnikoog are illustrated in Figure 4.12. As the residual transport of mud over the tidal divides is largely driven by meteorological variations such and wind and waves, these timeseries also show a strong seasonal variation. In addition, certain (storm) events lead to such large transport rates that these short events have a very large contribution in the total residual transport over a year.

Table 4.2 Model results of the total mud transport through the inlets of the Dutch Wadden Sea and over the tidal divide of Schiermonnikoog in 2017.

inlet or tidal divide	total import	total export	net import (+) or export (-)
Marsdiep	23 * 10^9 kg	21 * 10^9 kg	2.0 * 10^9 kg
Eierlandse Gat	5.9 * 10^9 kg	5.3 * 10^9 kg	0.67 * 10^9 kg
Vlie	27 * 10^9 kg	25 * 10^9 kg	1.5 * 10^9 kg
Borndiep	23 * 10^9 kg	25 * 10^9 kg	-2.0 * 10^9 kg
Friesche Zeegat	29 * 10^9 kg	30 * 10^9 kg	-0.56 * 10^9 kg
Schiermonnikoog	0.23 * 10^9 kg	2.0 * 10^9 kg	-1.7 * 10^9 kg
Total	108 * 10^9 kg	108 * 10^9 kg	-0.10 * 10^9 kg

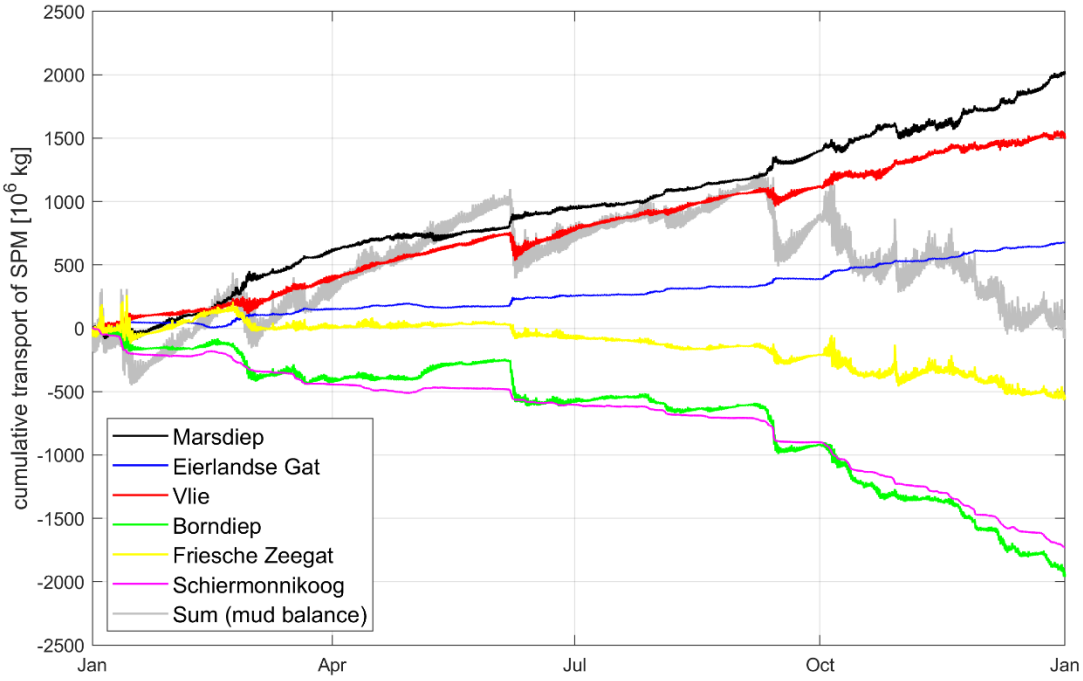

Figure 4.11 Model results of the cumulative mud transport through the tidal inlets and over the tidal divide of Schiermonnikoog in 2017. Positive transports are directed into the Dutch Wadden Sea.

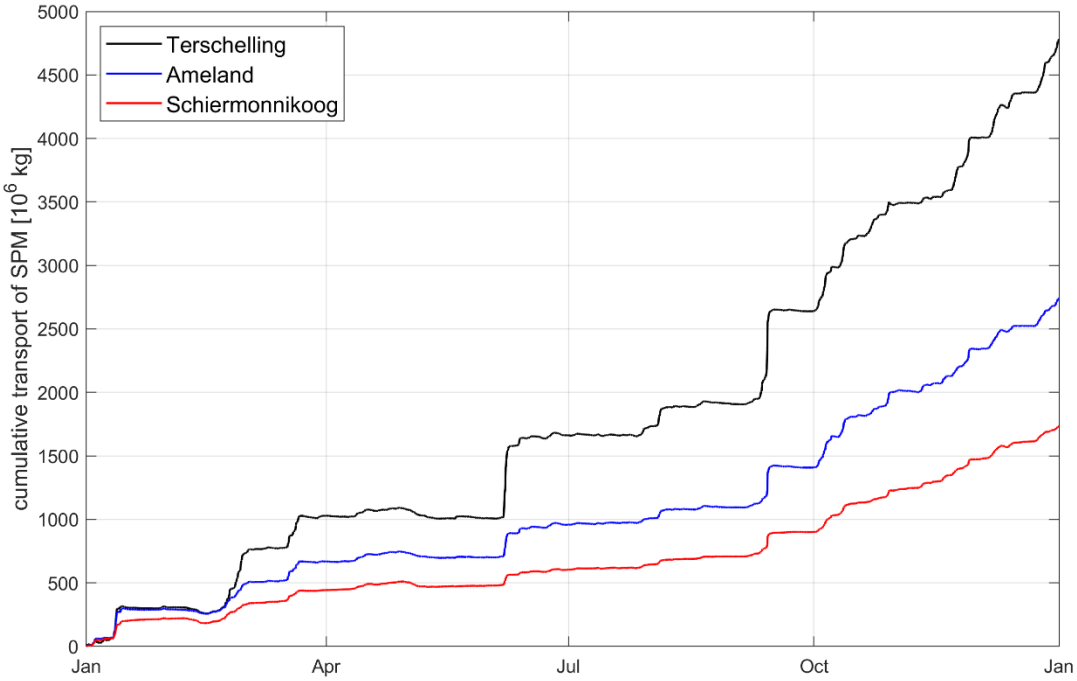

Figure 4.12 Model results of the cumulative mud transport over the tidal divides of Terschelling, Ameland and Schiermonnikoog in 2017. Positive transports are directed towards the east.

5 Conclusions and recommendations

5.1 Background

Upon request of Rijkswaterstaat (RWS), Deltares has developed a sixth-generation hydrodynamic and fine sediment transport model of the Dutch Wadden Sea (DWSM). The development of the present model is part of a more comprehensive project in which sixth-generation models were developed for all waters managed and maintained by RWS. An important difference with the previous fifth-generation models is the use of the D-HYDRO Suite, the new software framework for modelling free surface flows, which was first released in 2015 and allows for the use of unstructured grids.

Initially, the idea was to base the hydrodynamic DWSM model on a cut-out of the horizontal schematization of DCSM-FM 100m. Later this was coarsened to a resolution of ~200m to achieve a better balance between accuracy and computational burden. Despite the difference in model resolution, the spatially varying roughness was taken from DCSM-FM 100m (2022 release). The boundary conditions are obtained from nesting in 3D DCSM-FM (2022 release). The latter model also provides the numerical and physical settings, even though the number of vertical layers was later reduced from 20 to 10.

5.2 Validation

5.2.1 General

The second release of the hydrodynamic DWSM model has been validated with respect to water levels (including a sub-division in tide and surge), currents and (residual) discharges, as well as salinity and temperature. In general, the model has improved significantly compared to the first release of DWSM. The conclusions with respect to the model validation are further elaborated in the section below.

The fine-sediment transport model (DWSM-Mud) is validated against field measurements of suspended sediment concentrations at different timescales. Although the hydrodynamic model has significantly improved compared to the first release of DWSM, the performance of the fine sediment transport model is similar to what it was in the first release.

5.2.2 Hydrodynamics

Water levels

DWSM was validated with respect to mean water levels, tide, surge and total water levels. This was done by comparison against tide gauge measurements at 25 stations. The quality of 3D DCSM-FM, DCSM-FM 100m and the previous release of DWSM was used as a benchmark. Based on this the following can be concluded:

- Total water levels errors are generally between 5-8 cm, with the lowest errors in the North Sea stations.
- The tidal error is generally between 4-5 cm. Exceptions are Den Oever buiten and West-Terschelling with tidal errors of around 9 cm. Upstream in the Ems-Dollard, in Emden and Pogum, the tidal error increases to 12 cm and 19 cm, respectively. Compared to 3D DCSM-FM, the tide quality of DWSM is equal or better in most stations. Results have mostly improved compared to the previous release of DWSM.

- The surge error generally varies between 4-6 cm, with the lowest in the North Sea and increasing towards the mainland coast and upstream the Ems-Dollard. The surge quality is generally equal or better than in 3D DCSM-FM. Results have mostly improved compared to the previous release of DWSM.
- Low water level representation has improved substantially in Harlingen and Schiermonnikoog, compared to the previous release. The quality of the low waters remains poor in Holwerd, due to a coarse representation of the bathymetry, in relation to the width of the channel towards Holwerd.
- Mean water levels are generally well represented, with a station-averaged bias of 1.5 cm and a standard deviation of bias between stations of 2.0 cm.

Currents

The reproduction of depth-averaged flow velocities was validated by comparison against flow velocities that were measured during Kustgenese 2.0 field campaigns around Ameland Inlet in 2017. Based on this the following can be concluded:

- Along the North Sea coast of the Wadden islands Terschelling and Ameland, longshore flow velocities are generally well represented. The RMSE of the velocity magnitude is around 10 cm/s. Cross-shore velocities are less accurate in DWSM. This suggests that certain processes that cause a cross-shore current are not (well enough) included in the model.
- At the ebb-tidal delta of Ameland Inlet, the magnitude of measured flow velocities is reproduced well (i.e., RMSE around 10 cm/s). Flow velocities in the main channel of Ameland Inlet are reproduced with an RMSE of 18 cm/s for the velocity magnitude.
- Temporal variations in flow velocities at the tidal divides due to tides and meteorology are reasonably well represented by the model. Flow velocities around low water are underestimated by the model, probably related to an overestimation of low water levels.

(Residual) Discharges

- Discharges through the tidal inlet of Ameland in DWSM were validated against field data of three 13-hour measurement periods in September 2017. DWSM is considered to reproduce the discharges within the accuracy of the measurements (overestimation of the integrated ebb- and flood volumes with 7-10%).
- Model results of the residual discharges through tidal inlets of the Wadden Sea are validated by comparison with results of earlier modelling studies, since field data of the residual discharges is absent. The comparison indicates that residual discharges in DWSM are similar to the results of other models.

Salinity

DWSM was validated in 9 stations with respect to sea surface salinity for the year 2017 and compared to 3D DCSM-FM. Based on this the following can be concluded:

- In general, the sea surface salinity in the North Sea part of the domain is well represented, with an RMSE of 0.3 – 0.4 psu in most stations. This is of comparable quality to 3D DCSM-FM.
- In the Wadden Sea part of the domain, errors are larger than in the North Sea. This can be explained by the larger temporal and spatial variability in this area. Compared to 3D DCSM-FM the quality has improved in all four stations.
- Compared to the first release of DWSM, the quality of salinity representation has improved in most stations.

Temperature

DWSM was validated in 9 stations with respect to sea surface temperature for the year 2017 and compared to 3D DCSM-FM. Based on this the following can be concluded:

- The sea surface temperature is well represented in the North Sea part of DWSM, with a quality that is comparable to 3D DCSM-FM. The exception is Rottumerplaat 3 km, which significantly improves. The RMSE values in the four North Sea stations are around 0.3-0.4 °C.
- Errors in the Wadden Sea are between 0.3 °C and 0.6 °C, which is slightly larger than in the North Sea, but still very good given the coarse resolution of the meteorological forcing. The DWSM quality with respect to sea surface temperature is similar to 3D DCSM-FM. Compared to the first release of DWSM, the improvement in quality is striking, with a reduction in RMSE by a factor of 3-4 (from 1.0-1.6 °C to 0.3-0.4 °C).

5.2.3 Fine sediment dynamics

Suspended sediment concentrations (SPM)
DWSM-Mud was validated against MWTL measurements in 2017 at twelve observation points in the Wadden Sea, the North Sea and the Ems-Dollard estuary, and against MWTL measurements from different years at these twelve and seventeen other observation points. Based on this, the following can be concluded:

- The performance of this second release of DWSM-Mud is similar to the performance of the first release of this model, which is described by Vroom et al. (2020).
- Time-averaged SPM are reasonably well reproduced by the model, both in the Wadden Sea and in the part of the North Sea that is included in the model domain.
- Time-averaged SPM are underestimated at locations in the Wadden Sea and Ems-Dollard estuary where the observed SPM are relatively high, such as near Holwerd. This is probably because certain (feedback) mechanisms that cause these high sediment concentrations are not included in the model. Observed seasonal variations in SPM, with relatively high SPM in winter and low SPM in summer, are also reproduced by the DWSM-Mud model results.

Intra-tidal variations in SPM were validated against measured timeseries of the SPM near Eemshaven and Boontjes. Although the phasing and asymmetry of tidal variations is similar to what is observed in the measurements, the amplitude of intra-tidal fluctuations is much smaller in the model results than in the measurements.

Mud balance of the Wadden Sea
Model results of the residual mud transport into and out of the Wadden Sea provide insight into large scale exchange flows and the mud balance of the Dutch Wadden Sea. These model results of a single year can hardly be validated against field data, as those data only provide insight into multi-year trends. The net result of import and export over a full year is small, such that the amount of mud in the Dutch Wadden Sea varies during the seasons but is at the end of the year similar to what it was at the start of the year.

5.3 Recommendations

5.3.1 Model setup and hydrodynamics (DWSM)

Update Baseline database with more recent bathymetric data
The Baseline database has not been updated with the most recent measurements for the shoals in the Eierlandse Zeegat, Vliestroom and Amelander Zeegat. Because of this, the model bathymetry in these areas was overwritten based on a simple average of a set of LiDAR measurements from 2016 and 2017. It is recommended to update the Baseline database with these data.

Investigate performance in western Wadden Sea
While the the M2 tide is generally well represented, notable exceptions are four stations in the western Wadden Sea (Oudeschild, Den Oever buiten, West Terschelling and Kornwerderzand), where M2 phase errors occur of up to -8° and M2 amplitude error of up to 5 cm. Since the cause of these relatively large deviations from measurements are unknown, it is recommended to investigate and potentially improve this.

Improve tidal boundary conditions
The station-averaged M2 phase error in DWSM is -1.4°, which is relatively large compared to the -0.5° error in DCSM-FM 100m, and suggests that improvements are possible. The relatively large error may be due to a bias in M2 phase in 3D DCSM-FM, from which the open boundary conditions are obtained. Another possibility is the use of a roughness field that is based on the higher resolution, two-dimensional DCSM-FM model, without recalibration. It is recommended to further investigate the source of this error. Possible solutions could be improving the M2 phase in 3D DCSM-FM or investigating the possibility to use nested water levels from DCSM-FM 100m instead.

Higher resolution meteorological forcing
The currently used meteorological forcing has a 0.25 degrees (~30 km) spatial resolution, which is very coarse compared to the relevant spatial scales in the Wadden Sea. Despite good results for sea surface temperature, it is recommended to explore the advantages of the use of a higher resolution meteorological product such as Harmonie (Bengtsson et al., 2017).

Physical examination for spatially varying bottom roughness
The currently used spatially varying bottom roughness is taken from the DCSM-FM 100m model, and originally created based on water level water level measurements, using an automatic calibration procedure within the open source data assimilation toolbox OpenDA. While this yields excellent results in terms of water levels and tides specifically, a thorough physical explanation for the spatial patterns found is lacking. It is recommended to look into possible physical explanations for the spatial roughness patterns found. Possible starting points are spatial patterns in suspended sediment concentrations (increasing from east to west and in landward direction in the Ems Estuary) and the presence of sand waves.

Further investigation of the reproduction of measured flow velocities
A comparison between measured and modelled flow velocities revealed that cross-shore flow velocities are poorly reproduced at a few of the observation points along the North Sea coast of the Wadden islands. In addition, peak flow velocities during storm conditions are underestimated. It is recommended to investigate the origin of these differences between the observations and the model. The local bathymetry and the vertical velocity profile are worth looking into regarding the cross-shore flow velocities. The meteorological forcing (e.g. quality and spatial resolution of data) and the parametrization of the atmospheric boundary layer are relevant regarding the peak flow velocities.

Additional salinity and temperature measurements
While validation results with respect to salinity and salinity are good, the spatial distribution of the measurements over the Wadden Sea domain is poor. It is therefore recommended to increase the spatial coverage. For water temperature in particular it is important to also include shallow locations, where due to the thin layers of water and the temporarily exposure of sediment to the air creates additional uncertainty in the parameterization of the various heat-fluxes.

5.3.2 Fine sediment dynamics (DWSM-Mud)

Although the hydrodynamic model has been significantly improved compared to the first release of DWSM, the set-up and performance of the fine sediment transport model is very similar to what it was in the first release (Vroom et al., 2020). There are however multiple opportunities by which the fine sediment transport model could be improved, which couldn't be implemented during this update because of the limited amount of resources that were available. The following improvements are highly recommended.

Calibration and validation with new measurements

Currently, there is more field data available for the calibration and validation of the fine sediment transport model than is used during the initial calibration and validation of the model in 2020. Since 2021, continuous timeseries of SPM are obtained at two permanent measurement stations near Holwerd and Ferwerd. In addition, continuous measurements of the SPM are carried out near the tidal divide of Ameland during two months in the 2023-2024 winter. It is recommended to improve DWSM-Mud by re-calibration and validation with these field data, in particular with respect of intra-tidal variations in SPM. Residual SPM transport and SPM concentration gradients are generated by a combination of asymmetries in settling-remixing in the water column and deposition-resuspension at the bed over multiple time scales (intra-tidal, neap-spring, seasonal). The new high-frequency long-term measurements make it better possible to quantify these asymmetries and adapt the model settings accordingly.

The availability and – as of recently – accessibility of remote sensing data provides new opportunities to validate model results of spatial variations in SPM. These spatial variations were now only validated with infrequent point measurements. The additional validation of SPM fields by remote sensing data could build upon the exploration of using remote sensing data for SPM in the Dutch Wadden Sea by Van der Heijden et al. (2022).

An important aspect of the hydrodynamic forcing for the resuspension of sediment is the calibration of wave-induced versus current-induced bed shear stresses. If the wave-induced bed shear stress is too high, this may overestimate resuspension in channels and result in mud-starved shallow areas. If it is too low, the mud sink towards sheltered areas may be too large, resulting in too low overall concentration levels. In the current version of the fine sediment transport model, the calibration is based on expert judgement of spatial gradients in total bed shear stresses (Vroom et al., 2020). However, the computed current-induced, wave-induced and total bed shear stresses are pending validation with observations at various water depths.

Improved process formulations

Improvements of process formulations are recommended on two points, i.e. 1. the addition of interactions between sediment fractions in the water column and 2. changing the formulations for sediment exchange between bed layers.

Ad 1. The present model includes two sediment fractions but excludes any interaction between both in the water column. Formulations are available to include these interactions, also including the influence of salinity, temperature, turbulence and organic matter. The new measurements make it better possible to assess if the model performance improves if these interactions are included.

Ad 2. The sediment transport model distinguishes two sediment layers in the bed, each with a different resistance against erosion. In the current version of DWSM-Mud there is no direct exchange of sediment between these two layers. Implementing these exchange rates, often referred to as burial and digging, could improve the model performance. In particular, the burial of fines to deeper layers with a larger resistance against erosion could be useful to schematize the consolidation and strength increase of mud deposits in sheltered areas over time. The original model calibration was primarily aimed at reproducing turbidity levels and not at

reproducing sediment deposition rates in navigation channels and on mud flats. However, recently we see many applications on sedimentation and dredging, for which the model was not developed. The recommended change in process formulation will increase the range of model applications.

Include dredging and disposal works

Intensive dredging of both sand and mud takes place in several navigation channels in the Dutch Wadden Sea. Large volumes of fine sediment are mobilized by dredging and disposal, such that they have a significant impact on the sediment dynamics of individual basins. Dredging and disposal have earlier been implemented in models of the navigation channels Holwerd-Ameland (Grasmeijer et al., 2021) and Boontjes (Smits et al., 2022). It is recommended to include dredging and disposal also in DWSM-Mud and investigate its impact on the sediment dynamics in the Wadden Sea as a whole.

Improved wave model

The fetch-limited wave model that is used to include wave stirring in DWSM-Mud is computationally efficient, but insufficiently accurate in the North Sea and in parts of the Wadden Sea with strong gradients in the bathymetry. As the efficiency of a SWAN wave model has improved by means to parallelize the computations, it is recommended to investigate what the costs (i.e. in terms of computation time) and benefits (i.e. in terms of results) of a SWAN wave model are.

Allignment with the mud transport model of the North Sea

Over the past few years, a 3D model for combined hydrodynamics and mud dynamics in the North Sea has been developed as well (DCSM-FM; Zijl et al., 2021). The set-up of the hydrodynamic models of the North Sea and Wadden Sea is well aligned, for example by obtaining hydrodynamic boundary conditions for DWSM by nesting in DCSM-FM. However, The DCSM-FM model could also be used to generate boundary conditions for suspended sediment concentrations and the calibration and validation of both fine sediment transport models could be further aligned, which is recommended for future releases.

Literature

Andersen, T.J., Lund-Hansen, L., Pejrup, M., Jensen, K.T. & Mouritsen, K.N. (2005). Biologically induced differences in erodibility and aggregation of subtidal and intertidal sediments: a possible cause for seasonal changes in sediment deposition. Journal of Marine Systems 55 (3/4), 123–138.

Bengtsson, L., Andrae, U., Aspelien, T., Batrak, Y., Calvo, J., de Rooy, W., ... & Køltzow, M. Ø. (2017). The HARMONIE–AROME model configuration in the ALADIN–HIRLAM NWP system. Monthly Weather Review, 145(5), 1919-1935.

Charnock, H. (1955). Wind stress on a water surface. Quarterly Journal of the Royal Meteorological Society, 81(350), 639-640.

Colina Alonso, A., van Maren, D. S., Elias, E. P. L., Holthuijsen, S. J., & Wang, Z. B. (2021). The contribution of sand and mud to infilling of tidal basins in response to a closure dam. Marine Geology, 439, 106544. https://doi.org/10.1016/j.margeo.2021.106544

Duran-Matute, M., Gerkema, T., & Sassi, M. G. (2016). Quantifying the residual volume transport through a multiple-inlet system in response to wind forcing: The case of the western Dutch Wadden Sea. Journal of Geophysical Research: Oceans(121), 7431-7454.

Grasmeijer, van Weerdenburg, R., van Kessel, T. (2021). Invloed baggerstrategie op slibconcentraties en baggervolumes vaarweg Holwerd-Ameland. Deltares report 11206799-006-ZKS-0001.

Groenenboom, J., (2021): Wijzigingen in DCSM t.o.v. eerder gebruikte versies t.b.v. ontwikkeling Waddenzeemodel. Deltares memo, 11206814-009.

Herman, P., van Kessel, T., Vroom, J., Dankers, P., Cleveringa, J., de Vries, B., & Villars, N. (2018). Mud dynamics in the Wadden Sea. Towards a conceptual model. Deltares report 11202177-000-ZKS-0011.

Hurdle, D.P. & Stive, R.J.H., 1989. Revision of SPM 1984 wave hindcast model to avoid inconsistencies in engineering applications. Coastal Eng., 12: 339-351.

Lellouche, J. M., Greiner, E., Le Galloudec, O., Garric, G., Regnier, C., Drevillon, M., ... & Le Traon, P. Y. (2018). Recent updates to the Copernicus Marine Service global ocean monitoring and forecasting real-time 1⁄12 high-resolution system. Ocean Science, 14(5), 1093-1126.

Minns, T., A. Spruyt & D. Kerkhoven (2022): Specificaties zesde-generatie modellen met D-HYDRO - Generieke technische en functionele specificaties. Deltares report 11208053-012-ZWS-0002.

Oost, A., Colina Alonso, A., Esselink, P., Wang, Z.B., van Kessel, T., & van Maren, B. (2021). Where Mud Matters – Towards a Mud Balance for the Trilateral Wadden Sea Area: Mud supply, transport and deposition. Wadden Academy report 2021-02. ISBN 978-94-90289-57-7.

Pawlowicz, R., Beardsley, B., Lentz, S. (2002). Classical tidal harmonic analysis including error estimates in MATLAB using T_TIDE. Computers and Geosciences 28 (2002), 929-937.

Pivato, M., Carniello, L., Moro, I. & D'Odorico, P. (2019). On the feedback between water turbidity and microphytobenthos growth in shallow tidal environments. Earth Surface Processes and Landforms 44, 1192-1206.

Rijkswaterstaat. (1998). Sedimentatlas Waddenzee. Rijksinstituut voor Kust en Zee.

Smits, B., Vroom J., van Weerdenburg, R., & Colina Alonso, A. (2022). Morfologie en onderhoud vaargeul Boontjes. Systeembegrip en scenario's. Deltares report 11208040-004-ZKS-0004.

Swart, D. H. (1974). Offshore sediment transport and equilibrium beach profiles. PhD thesis, Delft University of Technology, Delft, The Netherlands.

Van der Heijden et al. (2023). Hybrid modelling Suspended Matter in the Wadden Sea. Deltares presentation on project no. 11206887-012.

Van der Werf, J., Antonio Álvarez Antolïnez, J., Brakenhoff, L., Gawehn, M., Den Heijer, K., De Looff, H., Van Maarsseveen, M., Holzhauer, H., Mol, J.-W., Pearson, S., Van Prooijen, B., Santinelli, G., Schipper, C., Tissier, M., Tonnon, P.K., De Vet, L., Vermaas, T., Wilmink, R., De Wit, F., 2019. Datareport Kustgenese 2.0. Deltares Report 220339-015-ZKS-0004 (The Netherlands).

Van Kessel, T., Winterwerp, H., van Prooijen, B., van Ledden, M. & Borst, W. (2011). Modelling the seasonal dynamics of SPM with a simple algorithm for the buffering of fines in a sandy seabed. Continental Shelf Research, 31, S124-S134.

Van Weerdenburg, R., Pearson, S. G., van Prooijen, B., Laan, S., Elias, E., Tonnon, P.-K. & Wang, Z. B. (2021). Field measurements and numerical modelling of wind-driven exchange flows in a tidal inlet system in the Dutch Wadden Sea. Ocean & Coastal Management, 215, 105941.

Van Weerdenburg, R. & Hanssen, J. (2023). Fetch limited wave models and resulting bed shear stresses in D-Flow FM: Implementation and validation. Deltares report I1000641-011-OA-0001.

Vroom, J., Van Weerdenburg, R., Smits, B. & Herman, P. (2020). Modellering slibdynamiek voor de Waddenzee: Kalibratie voor KRW slib. Deltares report 11205229-001-ZKS-0001.

Zijl, F., & Groeneboom, J. (2020). Development of a sixth-generation model for the NW European Shelf (DCSM-FM 100m). Deltares report 11205259-004-ZKS-0001.

Zijl, F., Groenenboom, J. & Laan, S.C. (2021). Development of a 3D model for the NW European Shelf (3D DCSM-FM). Deltares, report 11205259-015-ZKS-0003.

Zijl, F., Laan, S.C., Emmanouil, A., Van Kessel, T., Van Zelst, V.T.M., Vilmin, L.M. & Van Duren, L.A. (2021). Potential ecosystem effects of large upscaling of offshore wind in the North Sea. Bottom-up approach. Deltares report 11203731-004-ZKS-0015.

Zijl, F. (2021). Gevolgen van uitzetten RWE in DCSM-FM 100m. Deltares, memo 11206814-004, Delft.

Zijl, F., Groenenboom, J., Laan, S., Zijlker, T. (2022a). DCSM-FM 100m: a sixth-generation model for the NW European Shelf (2022 release). Deltares, report 11208054-004-ZKS-0002, Delft.

Zijl, F., Groenenboom, J., Laan, S., Zijlker, T. (2022b). 3D DCSM FM: a sixth-generation model for the NW European Shelf (2022 release). Deltares, report 11208054-004-ZKS-0003, Delft.

A Comparison of flow velocity reproduction with the WadSEA-FM Ameland (Kustgenese 2.0) model

A different Delft3D-FM model of the Dutch Wadden Sea has been developed for morphological studies within the Kustgenese 2.0 project. This model is referred to as the WadSEA-FM Ameland model. The computational grid is aligned with the North Sea coast of the Wadden islands and contains multiple refinement steps until a maximum resolution of around 30-50 m in Ameland Basin. The set-up, calibration and validation of the WadSEA-FM Ameland model are discussed in Van Weerdenburg et al. (2021). The WadSEA-FM model is used in 2D and does not compute variations in salinity and temperature. Here, the reproduction of flow velocities at observation points around Ameland Inlet in DWSM is compared to the reproduction in WadSEA-FM results. The observation points, that were part of the Kustgenese 2.0 field monitoring, are shown in Figure A.1.

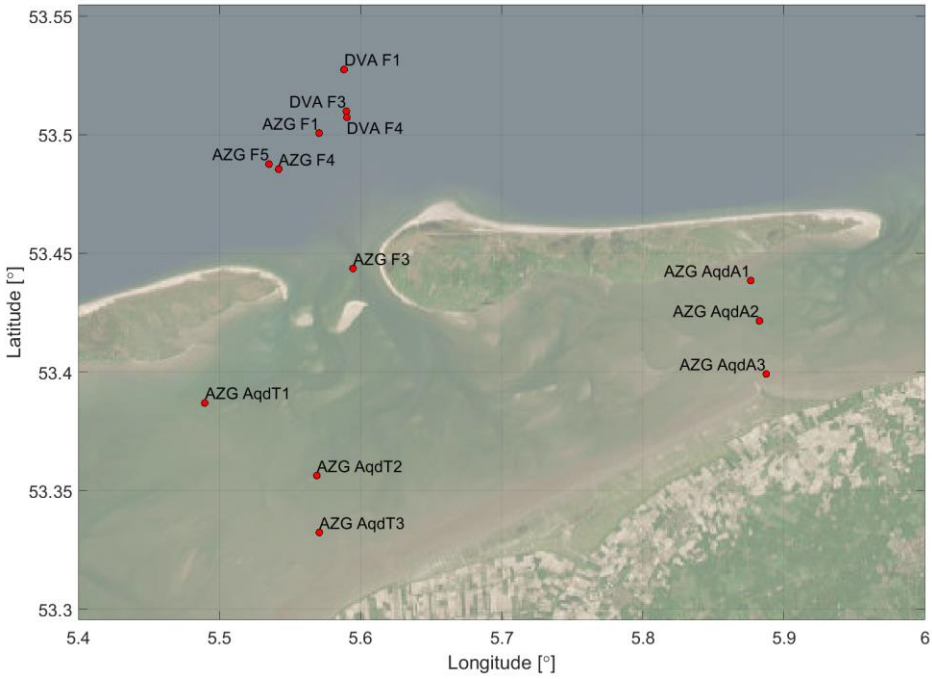

Figure A.1 Measurement locations for flow velocities during the Kustgenese 2.0 field campaings in 2017.

Characteristics of the reproduction of flow velocities in the tidal inlet and at the ebb-tidal delta are listed for both DWSM and WadSEA-FM in Table A.1 and Table A.2. For the observation points at the tidal divides of Terschelling and Ameland, the statistics are listed in Table A.3.

The comparison of results of DWSM and WadSEA-FM against field measurements indicates that the quality by which the two models reproduce the flow velocities around Ameland Inlet is similar. The statistics of the reproduction by DWSM are slightly better at some of the observation points, but at the same time slightly worse at other observation points. This spatial variation may be due to differences in bathymetry between both models, partly due to a difference in resolution.

Like in DWSM, the cross-shore currents at the lower foreshore are poorly reproduced by WadSEA-FM. The reproduction of flow velocities at the tidal divides is also similar between both models. A local difference between model bathymetries (i.e., observation point just in a small channel in WadSEA-FM and just next to a small channel in DWSM) makes that flow velocities at observation point AqdA2 are overestimated by WadSEA-FM.

Table A.1 Linear correlation coefficient (r) and root-mean-square error (RMSE) of the reproduction of measured depth-averaged flow velocity magnitudes at observation points around Ameland Inlet in DWSM and WadSEA-FM.

Station	**velocity magnitude**			
	DWSM		**WadSEA-FM**	
DVA lower shoreface	**r**	**RMSE [cm/s]**	**r**	**RMSE [cm/s]**
DVA F1	0.95	7.3	0.93	8.0
DVA F3	0.90	10.6	0.90	10.3
DVA F4	0.88	11.9	0.89	11.4
AZG ebb-tidal delta	**r**	**RMSE [cm/s]**	**r**	**RMSE [cm/s]**
AZG F1	0.93	8.8	0.90	9.2
AZG F3	0.94	18.2	0.79	25.1
AZG F4	0.86	12.6	0.86	11.4
AZG F5	0.88	10.5	0.88	10.4

*Table A.2 Linear correlation coefficient (r) and root-mean-square error (RMSE) of the reproduction of measured depth-averaged velocities at observation points around Ameland Inlet in DWSM and WadSEA-FM. * For unclear reasons, the flow direction of field measurements at observation point AZG F3 in the main channel of Ameland Inlet is not aligned with the orientation of the channel.*

Station	**u (west-east)**				**v (south-north)**			
	DWSM		**WadSEA-FM**		**DWSM**		**WadSEA-FM**	
DVA lower shoreface	**r**	**RMSE [cm/s]**	**r**	**RMSE [cm/s]**	**r**	**RMSE [cm/s]**	**r**	**RMSE [cm/s]**
DVA F1	0.99	8.3	0.99	8.3	-0.18	17.5	-0.13	17.3
DVA F3	0.97	12.7	0.97	12.7	0.44	14.6	0.65	13.2
DVA F4	0.94	18.0	0.94	16.8	0.65	19.9	0.80	18.1
AZG ebb-tidal delta	**r**	**RMSE [cm/s]**	**r**	**RMSE [cm/s]**	**r**	**RMSE [cm/s]**	**r**	**RMSE [cm/s]**
AZG F1	0.97	12.1	0.97	13.1	0.78	16.8	0.89	13.6
AZG F3*	0.52	29.6	0.48	16.9	0.99	14.9	0.96	27.3
AZG F4	0.96	13.1	0.97	12.6	0.74	11.6	0.74	9.8
AZG F5	0.97	11.5	0.97	10.9	0.22	13.4	0.27	12.8

Table A.3 Linear correlation coefficient (r) and root-mean-square error (RMSE) of the reproduction of measured depth-averaged flow velocity magnitudes at the tidal divides of Terschelling and Ameland in DWSM and WadSEA-FM.

Station	velocity magnitude			
	DWSM		WadSEA-FM	
AZG tidal divides	r	RMSE [cm/s]	r	RMSE [cm/s]
AqdT1	0.78	13.0	0.72	12.9
AqdT2	0.79	13.4	0.83	11.1
AqdT3	0.85	7.8	0.88	7.3
AqdA1	0.84	6.7	0.77	8.3
AqdA2	0.86	8.4	0.73	19.9
AqdA3	0.86	12.1	0.87	10.7

B Reproduction of observed wave parameters

Timeseries of the measured and computed wave height and wave period at Eierlandse Gat and at Nes are illustrated in Figure B.1 and Figure B.2, respectively. The timeseries illustrate that most of the variations in the wave parameters are reproduced well by the fetch-limited wave model. However, the wave period of small waves is generally underestimated. It was already found in an earlier validation of the fetch-limited wave model (Vroom et al., 2022) that wave heights in channels in the Wadden Sea are generally overestimated, because the local depth in the channels is larger than what would effectively be the fetch depth.

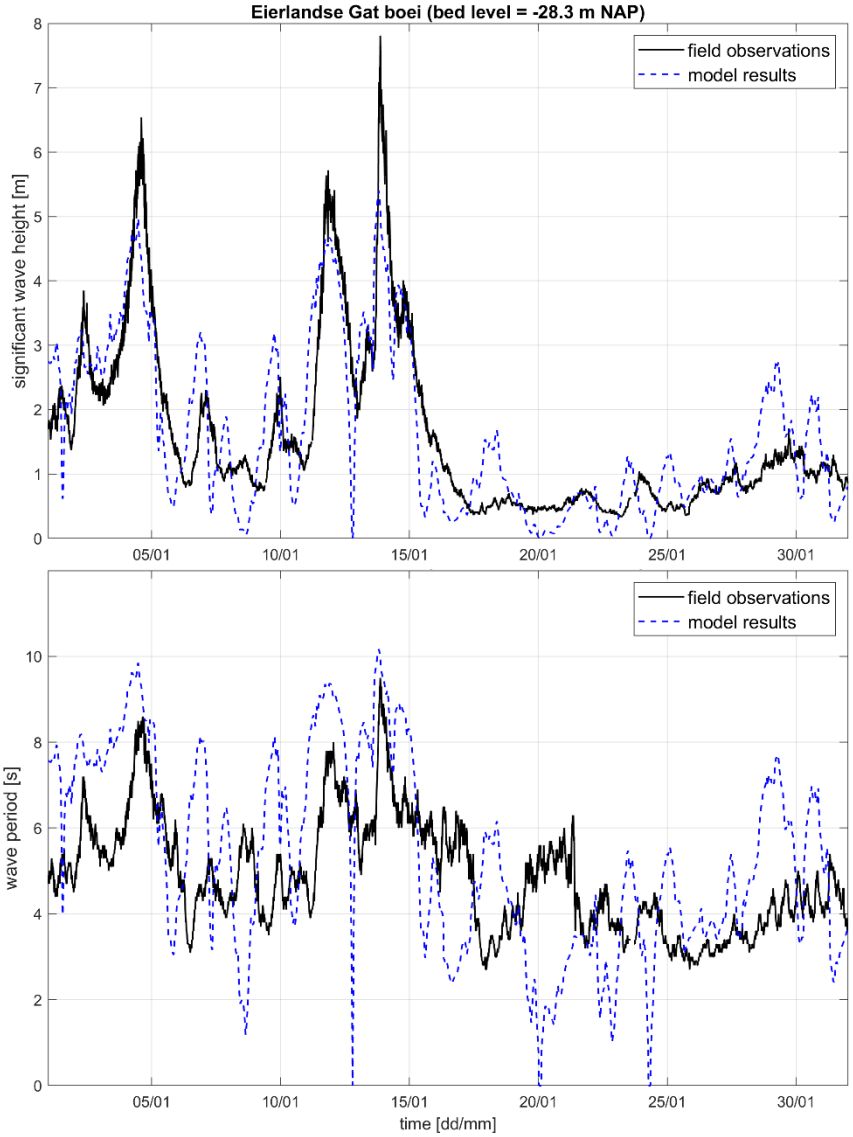

Table B.1 Field measurements and model results of the significant wave height (top) and wave period (bottom) at Eierlandse Gat in January 2017.

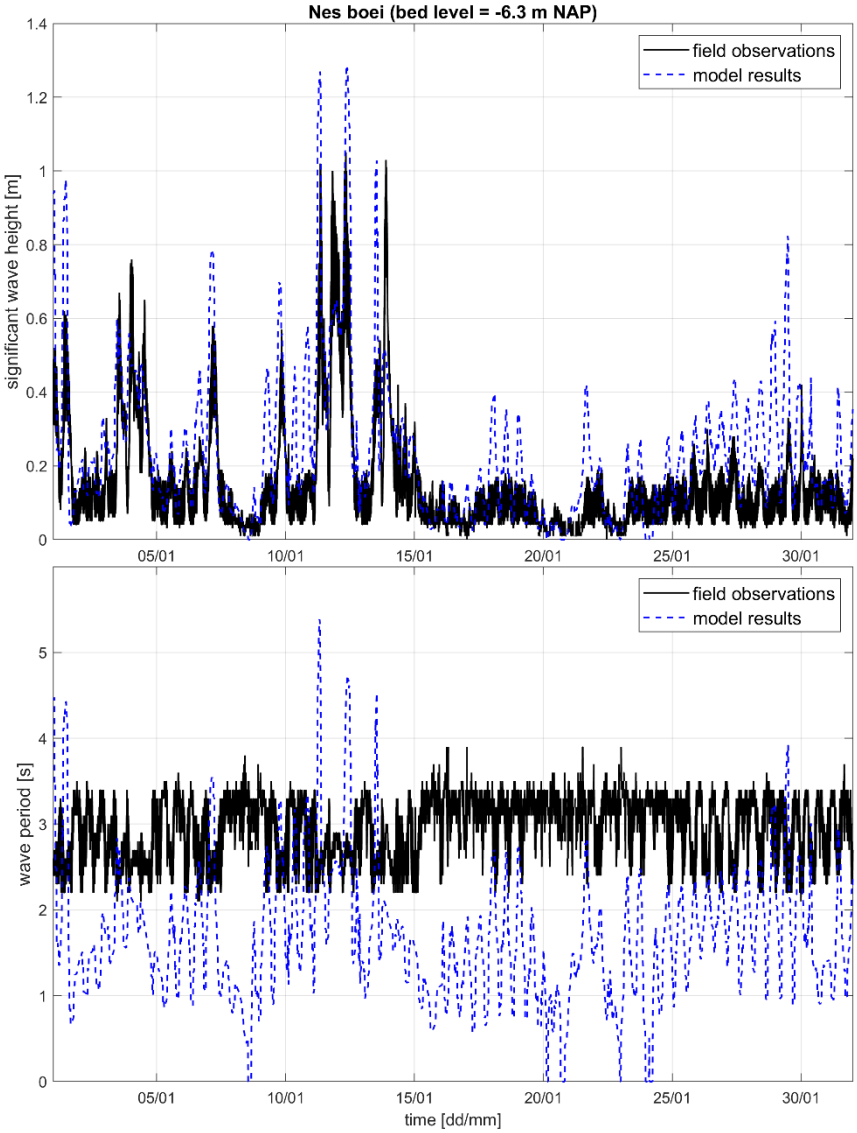

Table B.2 Field measurements and model results of the significant wave height (top) and wave period (bottom) at Nes in January 2017.

Deltares is een onafhankelijk kennisinstituut voor toegepast onderzoek op het gebied van water en ondergrond. Wereldwijd werken we aan slimme oplossingen voor mens, milieu en maatschappij.

Deltares

www.deltares.nl